J Comput Neurosci (2011) 31:419–440
DOI 10.1007/s10827-011-0319-y

Responses of a bursting pacemaker to excitation reveal spatial segregation between bursting and spiking mechanisms

Selva K. Maran · Fred H. Sieling · Kavita Demla · Astrid A. Prinz · Carmen C. Canavier

Received: 2 August 2010 / Revised: 15 February 2011 / Accepted: 16 February 2011 / Published online: 1 March 2011

Abstract Central pattern generators (CPGs) frequently include bursting neurons that serve as pacemakers for rhythm generation. Phase resetting curves (PRCs) can provide insight into mechanisms underlying phase locking in such circuits. PRCs were constructed for a pacemaker bursting complex in the pyloric circuit in the stomatogastric ganglion of the lobster and crab. This complex is comprised of the Anterior Burster (AB) neuron and two Pyloric Dilator (PD) neurons that are all electrically coupled. Artificial excitatory synaptic conductance pulses of different strengths and durations were injected into one of the AB or PD somata using the Dynamic Clamp. Previously, we characterized the inhibitory PRCs by assuming a single slow process that enabled synaptic inputs to trigger switches between an up state in which spiking occurs and a down state in which it does not. Excitation produced five different PRC shapes, which could not be explained with such a simple model. A separate dendritic compartment was required to separate the mechanism that generates the up and down phases of the bursting envelope (1) from synaptic inputs applied at the soma, (2) from axonal spike generation and (3) from a slow process with a slower time scale than burst generation. This study reveals that due to the nonlinear properties and compartmentalization of ionic channels, the response to excitation is more complex than inhibition.

Keywords Central pattern generator · Dynamic clamp · Phase response curve · Phase locking · Stomatogastric ganglion

Action Editor: Frances K. Skinner

Electronic supplementary material The online version of this article (doi:10.1007/s10827-011-0319-y) contains supplementary material, which is available to authorized users.

S. K. Maran · C. C. Canavier (✉)
Neuroscience Center of Excellence, LSU Health Sciences Center,
2020 Gravier Street, Suite D,
New Orleans, LA 70112, USA
e-mail: ccanav@lsuhsc.edu

F. H. Sieling
Department of Biomedical Engineering,
Georgia Institute of Technology and Emory University,
Atlanta, GA 30332, USA

K. Demla · A. A. Prinz
Department of Biology, Emory University,
Atlanta, GA 30322, USA

C. C. Canavier
Department of Ophthalmology, LSU Health Sciences Center,
2020 Gravier Street, Suite D,
New Orleans, LA 70112, USA

1 Introduction

Neurons that fire spontaneously and repetitively can be characterized by their phase resetting curves (PRCs), which tabulate the length of a cycle perturbed by an input as a function of when the input is delivered within the cycle. Endogenously bursting neurons have been shown to be important in well-studied invertebrate central pattern generators (CPGs) (Hartline 1979; Hartline and Gassie 1979; Miller and Selverston 1982; Tazaki and Cooke 1990; Arshavsky et al. 1989; Arshavsky et al. 1991; Nargeot et al. 1997; Nargeot et al. 2007), therefore we have focused here on endogenously bursting neurons, specifically in the pacemaker kernel of the pyloric circuit of the stomatogastric ganglion in crab and lobster.

The usual rationale for studying the phenomenology of phase resetting curves in bursting neurons is that they can be used to predict phase locking within a network (Oprisan et al. 2004; Sieling et al. 2009), with obvious utility to applications to central pattern generating circuits containing bursting neurons (Stein et al. 1997) and possibly to pathological network synchrony among bursting neurons in the case of epilepsy (Huguenard and McCormick 2007; Traub and Jefferys 1994) and tremor (Hammond et al. 2007). For bursting neurons, the duration and shape of the burst may change as a result of the feedback within a network, and synaptic strength may be modulated as well, thus it would be useful to understand how these changes impact the resetting (Demir et al. 1997; Oprisan et al. 2003), rather than generating PRCs for every possible scenario of burst truncation or elongation, and for every possible synapse strength. The bursting neuron in the study by Oprisan et al. 2003 was treated as a relaxation oscillator. This type of oscillator shows periodic activity tracing out a closed path, called a limit cycle, for each cycle in a space composed of voltage and a slow variable. The limit cycle for a bursting neuron, which can be characterized as a relaxation oscillator, has a depolarized (bursting) and hyperpolarized (silent) branch. Oprisan et al. 2003 showed that inhibitions applied during the burst produced a switch to the hyperpolarized branch, then prevented a switch back to the depolarized branch until the inhibition was turned off, whereas inhibitions during the silent phase had little effect. We characterized the response of bursting neurons to excitation rather than inhibition, and found the responses to excitation at the soma to be a very useful tool in probing the spatial localization and dynamics of burst generation. The PRC data was used to determine in very broad strokes the overarching principles governing how a model that captures the essential features of the PRC data should be organized. Our methods for understanding the phenomenology underlying observed PRCs should be generally applicable to bursting neurons (or groups of bursting neurons) that incorporate a relaxation oscillation as the burst generator.

Most CPGs, including the pyloric circuit, are dominated by inhibition (Calabrese and Peterson 1983; Marder and Calabrese 1996), but some also contain some excitatory connections (Cangiano and Grillner 2005; Cheng et al. 1998; McCrea and Rybak 2008). In CPGs such as the pyloric circuit, input perturbations are usually at least as long as the presynaptic burst duration, and burst durations are variable, so it is reasonable to examine the effect of input duration. In addition to our stated goal of understanding how the phase response of a bursting neuron to excitation changes as a function of synaptic strength and burst duration, part of the motivation for this work is to determine whether the phenomenology of inhibitory and excitatory phase resetting differs in fundamental ways that justify the predominance of inhibition in motor pattern generation. Indeed, in contrast to the previous work on inhibitory phase resetting, we found that there were five different PRC shapes exhibited in response to excitation, and that a more complex theoretical framework was required in order to interpret them.

2 Methods

2.1 Experimental methods

2.1.1 Electrophysiology

Somatic intracellular recordings of identified neurons from the pyloric network in the Stomatogastric ganglion of *Homarus americanus* and *Cancer borealis* were obtained using standard methods as in Sieling et al. 2009. The pacemaker is comprised of the anterior burster (AB) and the two pyloric dilator (PD) neurons to which it is electrically coupled. Since the AB/PD complex is electrically coupled and produces synchronous bursting activity (Abbott et al. 1991; Miller and Selverston 1982), we treated the AB/PD complex as a single oscillator or neuron. We pharmacologically isolated this group using 10^{-5} M bath application of Picrotoxin to block glutamatergic synapses.

2.1.2 Dynamic clamp used to generate artificial synapses

We recorded the membrane potential from one PD neuron (see Fig. 1(A)) and used the dynamic clamp (see Fig. 1(B)) (Prinz et al. 2004; Sharp et al. 1993a,b) to inject artificial synaptic inputs: the membrane potential V at the PD cell body was amplified, fed into a National Instruments DAQ board (PCI-6051E) and digitized at a rate of 20 kHz. In some experiments (see Table 1), AB rather than PD was impaled. The dynamic clamp program was written in C^{++} and designed to use the Real Time Linux Dynamic Controller (RTLDC) (Dorval et al. 2001). This program detected bursts in the ongoing PD rhythm and monitored the instantaneous period. Artificial synaptic inputs were generated and applied at different phases of the PD rhythm by instantaneously setting the synaptic conductance to the desired value for the desired duration. This was accomplished by injecting a current of the form $I_{syn} = g_{syn} s(V_{post} - E_{syn})$ where the activation variable s for the artificial synapse was zero before and after the pulse. During input, the program computed the momentary current. To inject this current into the PD neuron, the program computed the corresponding command voltage, which was turned into an analog voltage by the DAQ

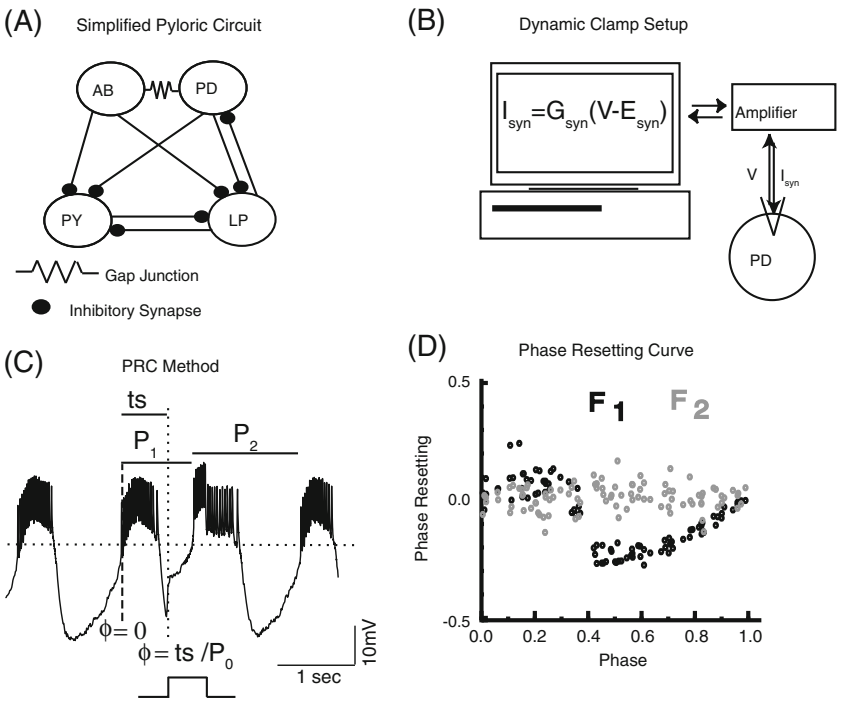

Fig. 1 Experimental setup. **(A)** Simplified pyloric circuit. The core pyloric circuit consists of nine to twelve neurons, which can be grouped as follows: the anterior burster neuron (AB), two pyloric dilator neurons (PD), five to eight pyloric neurons (PY), and one lateral pyloric neuron (LP). During experiments the only synaptic feedback to the pyloric pacemaker group through the LP to PD was removed by applying 10^{-5} M picrotoxin in the bath. (**B**) A schematic representation of the dynamic clamp experiment. A pharmacologically isolated AB/PD complex was impaled with a conventional sharp microelectrode via a single soma, and the membrane potential (V) recorded from that neuron (usually a PD neuron) is used to determine how much synaptic current (I_{syn}) this neuron receives through the artificial synapse. (**C**) Phase resetting measurement. The membrane potential record from an AB/PD complex, with an intrinsic period P_0, which is perturbed at the stimulus interval ts by an excitatory synaptic input. The peak of the first spike is designated as zero phase. The vertical dashed line corresponds to phase zero. The vertical dotted line indicates the time at which the input starts. P_1 corresponds to the period of the cycle in which the input starts and P_2 to the period of the next cycle. The dotted horizontal line at -45 mV is given for reference. (**D**) Phase Resetting Curve of a biological neuron (Neuron 6 in Table 1). F_1 (*black*) is first order resetting and F_2 (*gray*) is second order resetting. g_{syn}=20 nS, duration is 595 ms

board and sent to the electrode amplifier. In most cases (Table 1), we used either a square pulse in which s=1 for the duration of the pulse, or a slightly rounded square pulse with exponential rise and fall time constants of 10 ms as described in Sieling et al. 2009. In other cases (Table 2) we applied ramp inputs in which the conductance increased linearly during the input duration from s=0 to s=1, then reached its maximum value either at the end of the pulse (full ramp) or halfway through the input duration (half ramp). Our rationale for using ramps was that we thought that the depolarizing current injected by the dynamic clamp was opening voltage gated sodium channels located in between the soma and the burst generator in the dendrites, and we thought that if we depolarized gradually less of the current would be shunted into the extracellular space by these channels and more would travel axially toward the dendrites to depolarize them, but this approach was not successful.

2.1.3 PRC measurement

PRCs were generated by applying pulses of synaptic conductance to a single neuron within the complex, where the pulse was parameterized by conductance strength (10 to 250 nS, producing a peak in the PRC that can be as large as 100% of the intrinsic period of the isolated neuron) and duration (20 to 1,975 ms, ranging from 2% to 125% of the network period of the hybrid circuit). An important point is that this type of PRC does not assume that the magnitude of the PRC scales linearly with the strength of the perturbation, in contrast to the PRCs used in weak coupling theory (Ermentrout and Kopell 1991; Netoff et al. 2005; Preyer and Butera 2005). Instead, the dependence of the response on the strength and duration of the pulse is explicitly measured and definitely nonlinear. The simplifying assumption in this case is not that the coupling is weak, but that it is pulsatile (see Canavier and Achuthan 2010 for a review of pulse coupled oscillators).

Table 1 Summary of PRCs generated using a square pulse or slightly rounded square pulse

Neuron	Dur(ms)	Period (ms)			Strength (nS)									
		Min	Mean	Max	10	20	30	50	60	70	100	150	200	250
1	500	1251		1783	C	C		C/B			B			
2	20		1880			N		N			N			
	50					N		N			N			
	100					N		F			F			
	200					N					F			
3	50	1490		1702	N		N	N						
	100				N		F	F						
	200				N		F	F						
4(Crab)	50	598		745		F		F			F	F		
	100					F		F			F	F/B		
	200					F/B		B			B	B		
	500					C		T			T	B		
5	955		1097								U			
6	595	1271		1506		C			T					
	955					U			T		T			
7	695	1140		1204			C		B/T			T		
	955						U							
8(AB)	210		1602				N				F			
	1975						U							
9	100	796		847				N						
	500							C			C	C		
10	150	1529		1563				N				N	N	N
	500											B	B	B

The PRCs were divided into the following categories based on shape: F indicates prominent F_2 window, C cubic, B bilinear, U U-shaped, T trilinear and N stands for negligible. The totals for each category are as follows, with the number of neurons *n* that exhibited at least one PRC in the category is given in parentheses: F 15 (n=4), C 8 (n=5) B 8 (n=3) U 4 (n=4) T 6 (n=3) and N 19 (n=5). PRCs that were transitional between two categories totaled 4 (n=3) and are indicated by a slash between the two categories. All recordings were from lobster except neuron 4 which was from crab, and all recordings were from a PD soma except neuron 8 which was from AB. The input reversal potential used for Neuron 5 and Neuron 6 was 50 mV. For all other cases the reversal potential used was 0 mV. For Neurons 5 to 8 the synaptic input was a slightly rounded square pulse with exponential rise and fall time constants of 10 ms as explained in Section 2, in all other cases a square pulse was given. Since the period of the cycles changed slowly during recordings, the minimum (min) and maximum (max) values of the period are shown for some neurons. Dur corresponds to duration of the input

To generate the PRC of a biological neuron in response to a given synaptic input and for a given synapse strength g_{syn}, we first determined the intrinsic period P_0 of the biological neuron. Because the period of rhythm changed as we were recording, we used the average of the lengths of the cycles immediately preceding the three most recent inputs as the intrinsic period that determines the phase of the latest input (e.g., if the inputs are given during the 50th, 55th and 60th cycles, then the intrinsic period for the input given during the 60th cycle is the average of the periods of the 49th, 54th and 59th cycles). If the interspike interval preceding a given spike exceeded 50 ms in the case of lobster preparations and 75 ms in the case of crab preparations, this spike was considered to initiate a new burst, otherwise it was considered to be a continuation of an existing burst.

Once the intrinsic period was determined, the membrane potential of the biological neuron was recorded in response to conductance pulses of amplitude g_{syn} multiplied by a saved activation profile of the artificial synapse. Individual stimuli were delivered 10 s apart to ensure that the biological neuron returned to its unperturbed activity between stimuli. The stimulus interval (ts) was computed by multiplying the desired stimulus phase by the intrinsic period P_0. For a full PRC, we delivered stimuli at 100 equally spaced phases between 0 and 1. The order in which these stimuli were delivered was randomized. We took the peak of the first spike of the burst as the reference point and

Table 2 Summary of PRCs generated using a ramp input

Neuron	Dur (ms)	Period (ms)		Strength (nS)								
				60		80		100		150		200
		Min	Max	Full ramp	Half ramp	Full ramp	Half ramp	Full ramp	Half ramp	Full ramp	Half ramp	Full ramp
11	500	1450	1531			C	C					
12	50	990	1686		N			N	N/F		F	
	100			N/F	F			F	F	F	F	
	200							F	F	F		
	500			C				F/B	B	B	B	B

The synaptic inputs were given as ramps explained in Section 2. Briefly, the ramp is either given for full duration or for the first half (in the second half duration the neuron receives full strength input). The categories are the same as in table 1. All recordings are from PD somata in lobster. The totals are given as in the caption for Table 1; F 9 (n=1), C3 (n=2) B 4 (n=1) U 0, T 0 and N 2 (n=1). Three recordings from neuron 12 were transitional between two categories. The reversal potential used was 0 mV

assigned it to a phase of zero (see Fig. 1(C)). The first order resetting F_1 was defined as $(P_1 - P_0)/P_0$ and the second order resetting F_2 was $(P_2 - P_0)/P_0$, where P_1 is the period of the cycle in which the perturbation starts and P_2 is the period of the next cycle after perturbation onset (Fig. 1(C) and (D)).

2.2 Theoretical methods

2.2.1 Construction of multicompartmental model

The structure of the AB-PD complex is shown in Fig. 2(A). Each neuron in the complex has a soma, a primary neurite which gives rise to multiple dendrites, and an axon. The soma of the neuron receiving the dynamic clamp input was usually one of the two PDs, but occasionally it was AB instead. Similar activity was observed regardless of which neuron was impaled (see Table 1), and the illustrations consistently show the PD neuron as impaled. We used a four compartment model (assuming a PD neuron was impaled): a PD soma, a PD primary neurite, a PD axon and one lumped compartment for the combined dendrites of the two PD neurons and the AB neuron; a model schematic is shown in Fig. 2(B) and a circuit diagram in Fig. 2(C). The lumped dendritic compartment is justified by the connectivity of the dendrites of all the neurons in the pacemaker complex via gap junctions (Bucher et al. 2007). The somata, axons, and primary neurites of the neurons not impaled by the electrode were assumed to be too electrotonically distant to contribute to the activity observed at the impaled soma and were not included in the model. The essential feature of the model is the separation of the burst generating mechanism in the dendrites from the spike generating mechanism in the axon, which was accomplished by taking the currents from an earlier model (Guckenheimer et al. 1993) and separating them according to whether they contributed primarily to spiking or to generating the burst envelope.

The soma, as the locus of the current injected by the dynamic clamp, was retained as a separate compartment because in order to quantitatively model the data, we had to assume that the soma was distal to both spike and burst generation. The soma was considered to be passive and connected directly only to its own primary neurite, which was also essentially passive except for a slowly activating potassium conductance that was required to model the response to depolarizing pulses greater than a third of the intrinsic period. This hypothesized slow potassium current must be separated from the burst generator because it must be strongly coupled to or co-localized with spiking. The primary neurite was strongly coupled to the axon but only weakly coupled to the lumped dendrites. As a result both soma and axon have only weak interactions with the dendritic compartment. In summary, the synaptic input applied at the soma, the spiking currents in the axon, and a slow potassium current putatively located in the primary neurite all need to be separated from the burst generator in the dendrites. The axon, soma and primary neurite were separated to obtain a better quantitative fit to the data, however if only a qualitative fit were desired, the axon, soma and primary neurite could be combined into a single compartment for a minimum of two compartments.

Most of the ionic currents in the model were taken from previously published single compartment AB/PD complex model (Guckenheimer et al. 1993). All compartments have a membrane capacitance (C_m) in parallel with a leak current (I_L). The spiking currents, that is the fast sodium current (I_{Na}) and the delayed rectifier potassium current (I_{Kdr}), were taken directly from the previous model and inserted only in the axonal compartment. A small bias current I_{ext} was

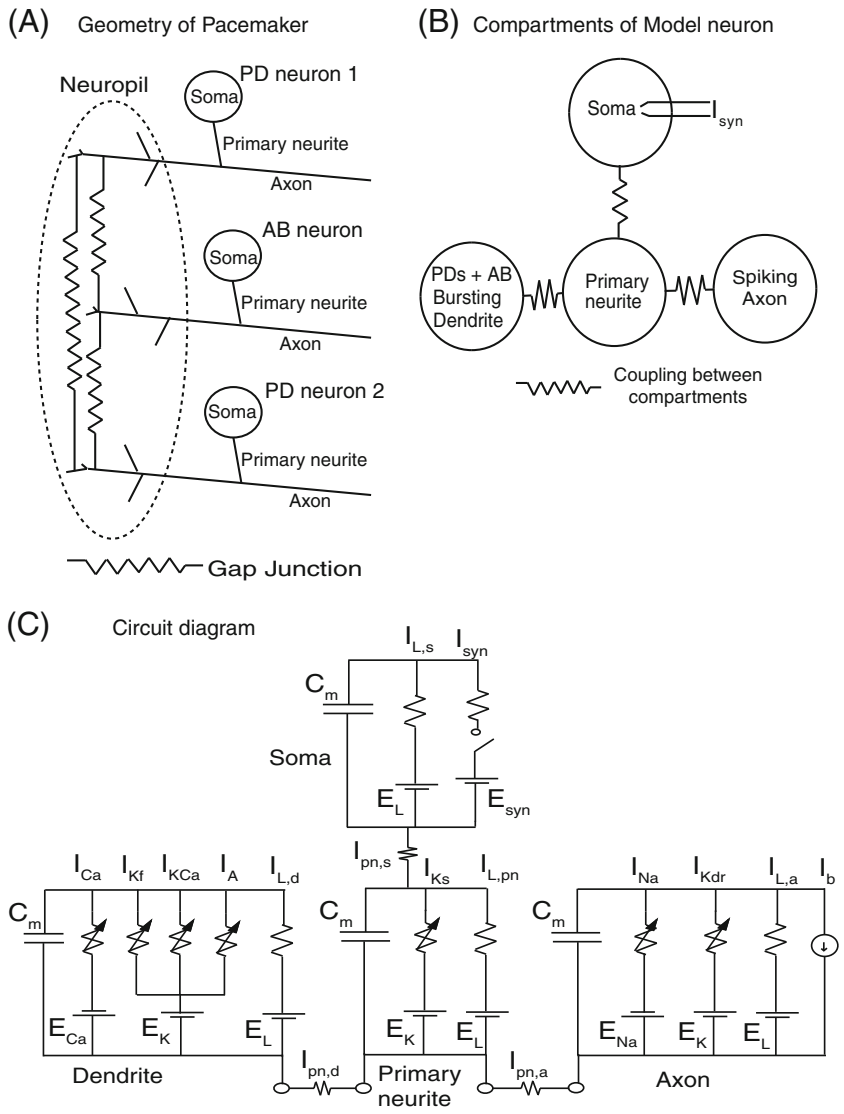

Fig. 2 Model formulation. (**A**) Schematic illustrating the geometry of pacemaker kernel. The dendrites of AB and two PD neurons are connected through gap junctions and comprise the neuropil. (**B**) Schematic of the model neuron. It has four compartments corresponding to PD soma, primary neurite and axon of the injected neuron and a lumped dendritic compartment (indicated by dashed ellipse in panel (A)). Sometimes the injected neuron is AB instead of PD (see Table 1). (**C**) Circuit diagram

added to the axon compartment to improve the fit to the data. On the other hand, the currents that are the primary determinants of bursting activity were taken directly from the earlier model and inserted in the lumped dendritic compartment. These currents were primarily the slowly voltage-activated and calcium-inactivated calcium current (I_{Ca}) and the calcium -activated potassium current (I_{KCa}), with a lesser contribution from the A-type potassium current (I_A). A fast potassium current (I_{Kf}) was added to the dendritic compartment to improve the correspondence of the model with the actual PRCs, mostly for the inhibitory case which was considered for consistency with our previous studies (Oprisan et al. 2003). The burst mechanism consists of a slow accumulation of calcium entry via the slow calcium current which is eventually terminated by the calcium-activation of a potassium current as well as by the calcium inactivation of the calcium current, and reinstated after a hyperpolarization in which the calcium concentration decays sufficiently to restart the depolarizing phase. Due to the strong coupling of the axon to the primary neurite, any depolarization of the primary neurite produces spiking in the axon, regardless of whether the depolarization originates from the synaptic input applied to the soma or from the up state of the burst generator in the soma. Although other currents are known to be expressed in the AB/PD complex, we present here only the minimal model required to provide a convincing fit to the experimental data. The most notable omission is the hyperpolarization activated current I_H (Tohidi and Nadim 2009), but the leak current I_L has similar effects on the resetting curve as I_H (Prinz et al. 2003b). The full set of model equations is given in Appendix A with parameter values as in Table 3.

The model PRCs were calculated using the same protocol as for the biological neurons. The model is

implemented in C and uses a fourth order Runge–Kutta method with a fixed step size of 0.02 ms. The simulations were done using a Scyld Beowulf Computational Cluster with CentOS 4.0 and AMD Opteron 280 processors. The cluster is a 64 bit machine with a Pathscale compiler.

2.2.2 Phase plane and nullcline analysis

In order to visualize what happens during the application of a pulse, a two-dimensional projection of the 11 dimensional full state space of the model was plotted in a phase plane consisting of the rapidly varying dendritic membrane potential V_d and a slow variable, the dendritic calcium concentration c. The voltage nullcline for an isolated dendritic compartment consists of the pairs of values of dendritic membrane potential and dendritic calcium concentration at which the rate of change of dendritic membrane potential is zero. The nullcline was calculated by determining at each value of dendritic potential V_d, the value of Ca^{2+} that made the following expression equal to zero: $I_{L,d}(V_d)+I_{K,Ca}(c, V_d)+I_{Ca}(z(V_d), c, V_d)+I_A(m_A(V_d), h_A(V_d)+I\ K_f(b(V_d), V_d)$ with all gating variables z, m_A, h_A and b set to their steady state value (indicated by the dependence of the gating variable on V_d) at the value of V_d. The isolated dendrite was examined because during a normal bursting cycle, the coupling currents are quite small and brief (Supplemental Figure 1), therefore their inclusion would complicate the analysis but provide no additional insights.

Table 3 Parameter values

Par	Values	Units	Par	Values	Units
ρ	0.0016	ms^{-1}	$G_{L,d}$	0.0354	μS
λ_n	0.8	ms^{-1}	$G_{L,pn}$	0.001	μS
λ_h	0.8	ms^{-1}	$G_{L,s}$	0.001	μS
K_A	1	ms^{-1}	$G_{L,a}$	0.001	μS
τ_z	23	ms	G_K	8.0	μS
τ_b	1	ms	G_{Ca}	0.04	μS
K_{Ca}	0.0078	mV^{-1}	G_{Na}	15.0	μS
z_b	−50	mV	G_{sK}	0.065	μS
v_a	−12	mV	G_{Kf}	0.07	μS
v_b	−62	mV	G_A	100	μS
s_a	−26	mV	G_{KCa}	0.273	μS
s_b	6	mV	C_m	1.0	nF
E_{Na}	30	mV	I_{ext}	0.2	nA
E_{Ca}	140	mV	$G_{s,pn}$	0.05	μS
E_K	−75	mV	$G_{a,pn}$	0.5	μS
E_L	−40	mV	$G_{d,pn}$	0.04	μS

3 Results

The PRCs recorded from pyloric pacemaker kernels depended upon the strength of the synaptic conductance as well as upon the duration of the perturbation. With respect to the strength of the perturbation, we define strong pulses as those that immediately evoked spiking regardless of phase, and weak pulses as those that do not evoke spiking unless they are applied during a burst when spiking is ongoing in any case. With respect to duration, by our definition a short pulse lasts less than one sixth of the intrinsic period of the neuron, an intermediate pulse lasts one sixth to one third of the period, and a long pulse lasts longer than a third of the period. For comparison, a burst generally occupies around a third or so of the period. Since we varied both the strength and duration of the pulse, the PRCs were roughly grouped into six categories. The short, weak pulses had no measurable effect. In the next five sections, we summarize the five characteristic PRC shapes that we observed corresponding to the other five categories. The model described in the methods produced PRCs that were strikingly similar to the experimentally observed PRCs. This indicates that the model captures essential features of the dynamics of the biological oscillator, and allowed us to formulate hypotheses regarding why these characteristic shapes were observed.

3.1 PRC with a prominent F_2 window

Short, strong pulses produced the characteristic PRC shape shown in Fig. 3(A1) (experimental data) and Fig. A2 (model), with the first order PRC given in black and the second order in gray. In both cases, excitatory pulses applied during a burst, not surprisingly, have little effect, hence both biological and model PRCs are essentially zero for early phases. The arrows labeled B and C in Fig. 3(A2) indicate two distinct regions in the PRC. Region B shows the eponymous "window" of phases (here from about 0.45 to 0.65) in which the second order resetting (F_2, shown in gray) is distinctly nonzero. After the burst has terminated, an excitatory pulse has the apparent effect of initiating a new burst when observed at the soma in both the biological (Fig. 3(B1)) and model (Fig. 3(B3)) neuron. Since we define the start of a burst by the onset of spiking, pulses given in this window shorten two observed burst cycles (F1 and F2) by about half a cycle each, so the "two" cycles together have the length of a single unperturbed cycle. Therefore the timing of the next burst after the pulse is essentially unchanged, which caused us to suspect the "burst" observed during the pulse itself was spurious. If the sum of the first and second order resetting is zero (modulo one), then there is no permanent resetting (Winfree 1980). Our hypothesis is that bursting is driven by a slow

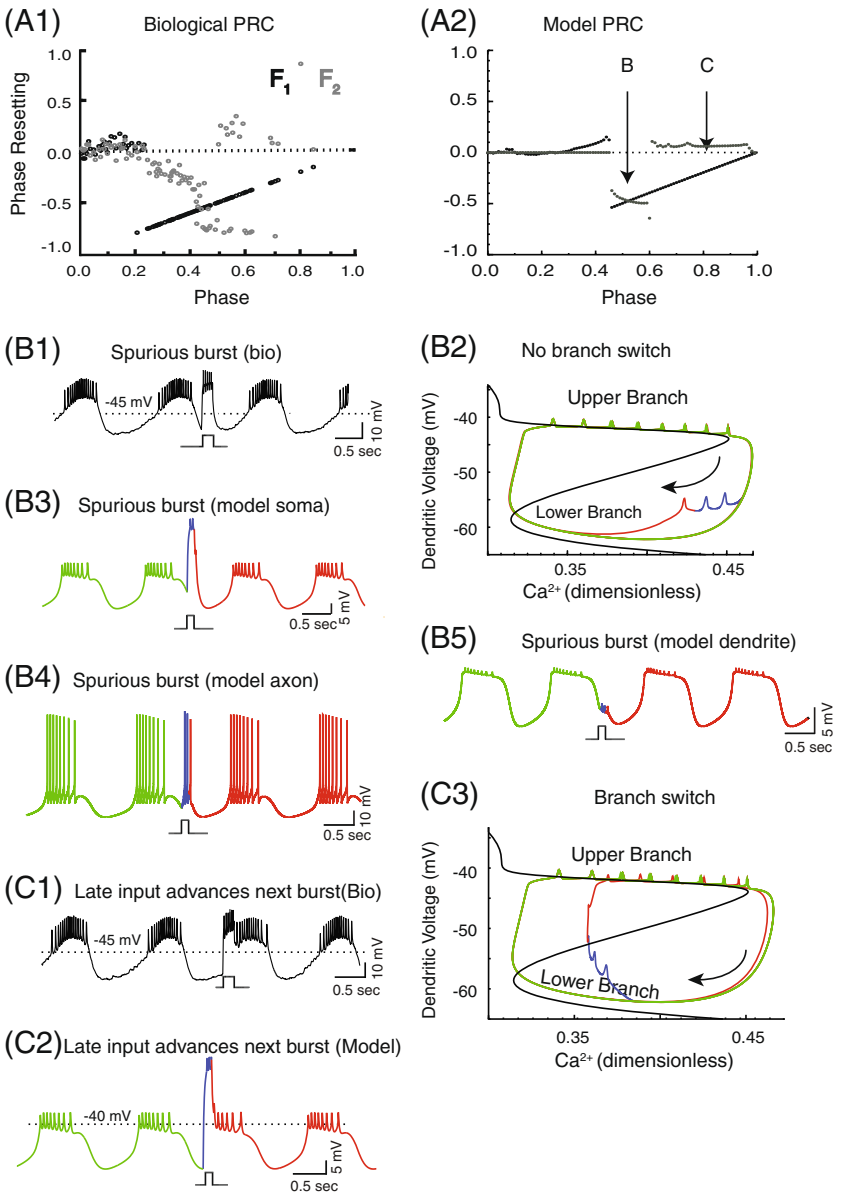

Fig. 3 Prominent F_2 window PRC for short strong cases explained. (**A**) Biological (A1) and model (A2) PRCs, with first order in black and second order in gray. The arrows indicate the regions of the PRC that correspond to panels B and C. (**B**) Voltage traces recorded at the soma for a pulse given early in the interburst interval show a shortened cycle initiated by the pulse for the biological (B1) and model (B3) neurons. (A1) The biological neuron is Neuron 3 (G_{syn}= 50 ns, duration=200 ms) in Table 1. (B2 and B3) In the model neuron, an input strength of 60 nS is applied for 125 ms. The green trace is unperturbed, the blue trace is during the pulse (pulse shown below voltage trace) and red trace is after pulse offset. Dendritic phase plane analysis (B2) shows that there is no transition to the upper branch. The arrow shows the direction of flow. The membrane potential in the axonal compartment (A4) shows that axonal spikes are evoked throughout the pulse, but do not reflect a new plateau in the dendritic membrane potential (A5), which is unaffected except for small spikelets that occur during the pulse. (**B**) Voltage traces recorded at the soma for a pulse given applied later in the interburst (B1 and B2) show that the cycle initiated by the pulse is not shortened. The phase plane analysis (B3) shows that in this case, there is nonetheless a premature transition to upper branch. The black curve is the voltage nullcline

oscillation in the dendrites that periodically depolarizes the axonal compartment sufficiently to generate a burst of spikes, then hyperpolarizes during the interburst interval. The model shows that the pulse-induced burst merely reflects spikes in the axonal compartment (Fig. 3(B4)) evoked directly by the somatic depolarization, and did not reflect a switch to a plateau in the dynamics of the dendritic burst generator (Fig. 3(B5)). The coupling between soma, dendrite and axon is clearly weak as evidenced by the disparity of the waveforms in panels 3B3-5, and this is

critical to produce the PRC shape in Fig. 3(A2). Unless the full depolarization induced by either the depolarizing conductance injected at the soma or the resultant spikes in the axonal compartment is greatly reduced in the burst generating compartment by weak coupling between the depolarized compartments and the dendritic burst generator, a depolarizing pulse in the soma would always induce a switch to the upper branch in the dendrite, contrary to experimental observation and underscoring the need for separation of these processes (see Supplemental Figure 2) from the burst generator.

The dynamics of the model dendritic burst generator are those of a relaxation oscillator, as we explain using the phase plane analysis in Fig. 3(B2). We plot projections of the full state space onto the Ca_d^{2+}-V_d plane, as described in Section 2. In Fig. 3(B2), this produces a trajectory in which time progresses in the direction of the arrow. The green curve represents the repetitive periodic path, or limit cycle, traced out by the bursting oscillation in this plane. In a relaxation oscillator, the trajectory spends most of its time either on the upper branch of the limit cycle corresponding to the plateaus in Fig. 3(B5) or on the lower branch corresponding to the troughs, with relatively quick jumps between branches. Our expectation was that strong short pulses would produce a burst by initiating a jump to the upper branch, but there is no premature switch to the upper branch of the limit cycle, either during the pulse (blue trace in Fig. 3(B2)) or after pulse offset (red trace in Fig. 3(B2)). However, during the pulse, small spikelets can be observed in the dendritic compartment (Fig. 3(B2) and (B5)) passively following the axonally generated spikes.

The window of prominent F_2 is terminated when the pulse is applied late enough in the interburst so that the spurious burst merges seamlessly into the next regularly scheduled burst (arrow C in Fig. 3(A2)) corresponding to the voltage traces in the somatic biological neuron (Fig. 3(C1)) and model neuron (Fig. 3(C2)). Interestingly, this case does show a delayed switch to the upper branch, but it is not evident without the phase plane analysis shown in Fig. 3(C3). The voltage nullcline (black curve) was calculated for an isolated dendritic compartment by setting the gating variables to their steady state values and finding the pairs of values of dendritic membrane potential and dendritic calcium concentration that result in zero net current flow across the dendritic membrane. There are three branches to this nullcline; the middle branch represents a forbidden zone that repels trajectories (Rinzel and Ermentrout 1989) and so crossing this boundary during the pulse (blue trace in Fig. 3(C3)) forces a branch switch between the lower and upper branches as shown after pulse offset (red trace). There is no F_2 in this case because only a single observable cycle is shortened in this case in contrast to two in the case illustrated by Fig. 3(B1 and B2). Note that for the biological neuron, there is a range of phases (~ 0.5–0.7) for which either of these outcomes is possible, depending upon trial to trial variability. The key insight is that the position of the trajectory relative to the middle branch of the limit cycle at pulse offset determines whether the trajectory will decay back to the lower branch (case B) or keep going toward the upper branch (case C). Thus the middle branch acts as a separatrix between the upper and lower branches. The linear segment with an approximate slope of one at late phases for all strong pulse cases reflects the immediate initiation of a burst at a phase of ϕ, resulting in an advance with a magnitude equal to the remainder of the cycle ($1-\phi$), but with opposite sign ($\phi-1$). This line segment is known as the causal limit, because an input cannot advance the next burst time any further, or the burst would occur before the input that caused the advance, in violation of causality. Analytical expressions for the linear segments of the phase resetting curves are given in the summary section below.

3.2 Cubic PRC

Weak pulses of intermediate duration given at phases during the burst generally produce a first order PRC that has the approximate shape of a cubic polynomial with zeros at zero, ϕ_b, and one, where ϕ_b is the phase at which burst termination occurs in both biological (black trace in Fig. 4(A1)) and model (black trace in Fig. 4(A2)) neurons. The arrow B in Fig. 4(A2) indicates a region of early phases in which delays predominate, and the arrow C a region of late phases in which advances predominate. Second order resetting (gray traces) is negligible for cubic PRCs. Fig. 4(B) shows an example of delays at early phases, whereas Fig. 4(C) illustrates advances at late phases for both the biological (Fig. 4(B1, C1)) and model neuron (Fig. 4(B2, C2)). The phase plane analysis in Fig. 4(B3) shows that during the pulse (blue trace), the trajectory remains on the upper branch for two additional spikes at the end of a burst, resulting in delays for perturbations applied during a burst. The same input applied during the interburst advances the time of the next burst by causing a switch from the lower branch to the upper branch during the perturbation (Fig. 4(C3), blue trace) at an earlier point on the limit cycle compared to the unperturbed trajectory (green). At intermediate phases, the perturbation both extends the burst and shortens the interburst, so the phase resetting is determined by the net effect of the delay and advance, producing a smooth transition from delay to advance in the cubic PRC shape. Note that for neurons with cubic PRCs, in contrast to those with prominent F_2 windows, the presence of spikes during the perturbation signals that the trajectory is on the upper branch and the absence of spikes signals that the trajectory is on the lower

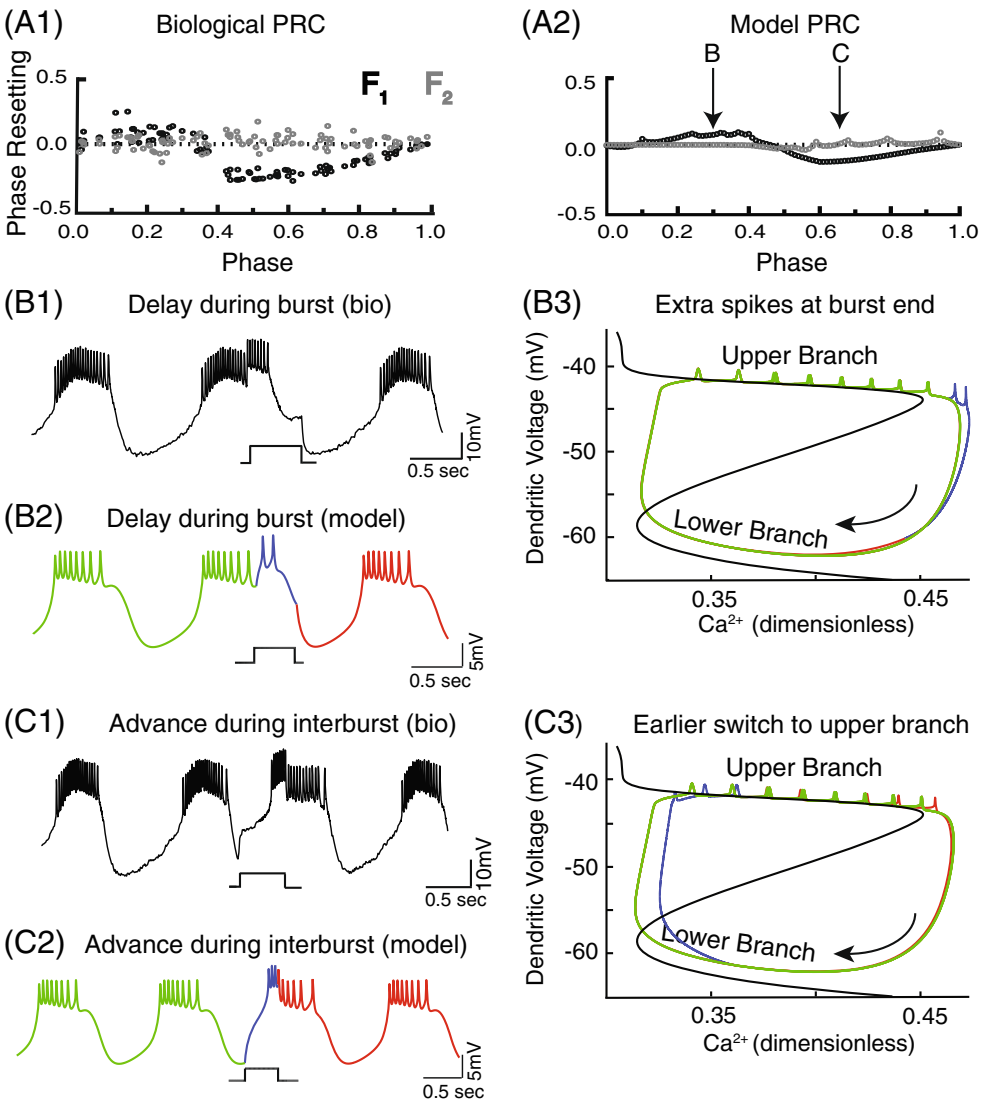

Fig. 4 Cubic PRC for intermediate, weak pulses explained. (**A**) Biological (A1) and model (A2) PRCs, with first order in black and second order in gray. The arrows indicate the regions of the PRC that correspond to panels (B) and (C). (**B**) Voltage traces recorded at the soma for a pulse given during burst for the biological neuron (B1) and the model neuron (B2). The phase plane analysis (B3) shows that some spikes are added to the burst, producing a delay. (**C**) Voltage traces recorded at the soma for a pulse given during interburst for the biological neuron (C1) and the model neuron (C2). The dendritic phase plane analysis (C3) shows that an earlier shift to the upper branch causes the advance. The colors and curves in model neuron voltage trace and phase plane analysis correspond to those in Fig. 3. In the model neuron, an input strength of 5nS is applied for 400 ms. The biological neuron is neuron 6 (G_{syn}=20nS, duration=595 ms)

branch. This correlation holds in general only for weak inputs, because weak inputs, unlike strong ones, cannot directly evoke spikes in the axonal compartment.

3.3 Bilinear PRC

Strong pulses of intermediate duration, like weak ones, also produce early delays and late advances for both biological (Fig. 5(A1)) and model (Fig. 5(A2)) neurons. Instead of a cubic shape, however, there is an apparent discontinuity (Glass and Winfree 1984) rather than a smooth transition between the regions of delays (arrow B in Fig. 5(A2)) and advances (arrow C in Fig. 5(A2)), resulting in two discontinuous line segments that produce a bilinear shape. For the cubic PRC case described above, transitions between the upper and lower branches occurred spontaneously during the input conductance pulse. In contrast, for the bilinear PRC case, the strong input forces spiking to persist throughout the pulse. For pulses applied during the burst, this persistent spiking prolongs the duration of the burst until pulse offset, such that the later the pulse starts, the greater the delay. On the other hand, the time from pulse offset until the next burst is approximately constant. This produces the first line segment in the bilinear PRC (Fig. 5 (A)) in which the delay varies linearly with phase. The reason for the constant rebound until the next burst is that the trajectory in the phase plane (Fig. 5(B3)) converges on a relatively compact region of phase space (black oval) during the tonic spiking induced by the conductance pulse (blue curve). No matter how many spikes are emitted during the burst, the path taken after pulse offset (red trace) is predictably constant since the trajectory always starts from approximately the same point and quickly relaxes back to the unperturbed limit cycle, producing the next burst in about the same amount of time from pulse offset each time. If the very slowly activating potassium current

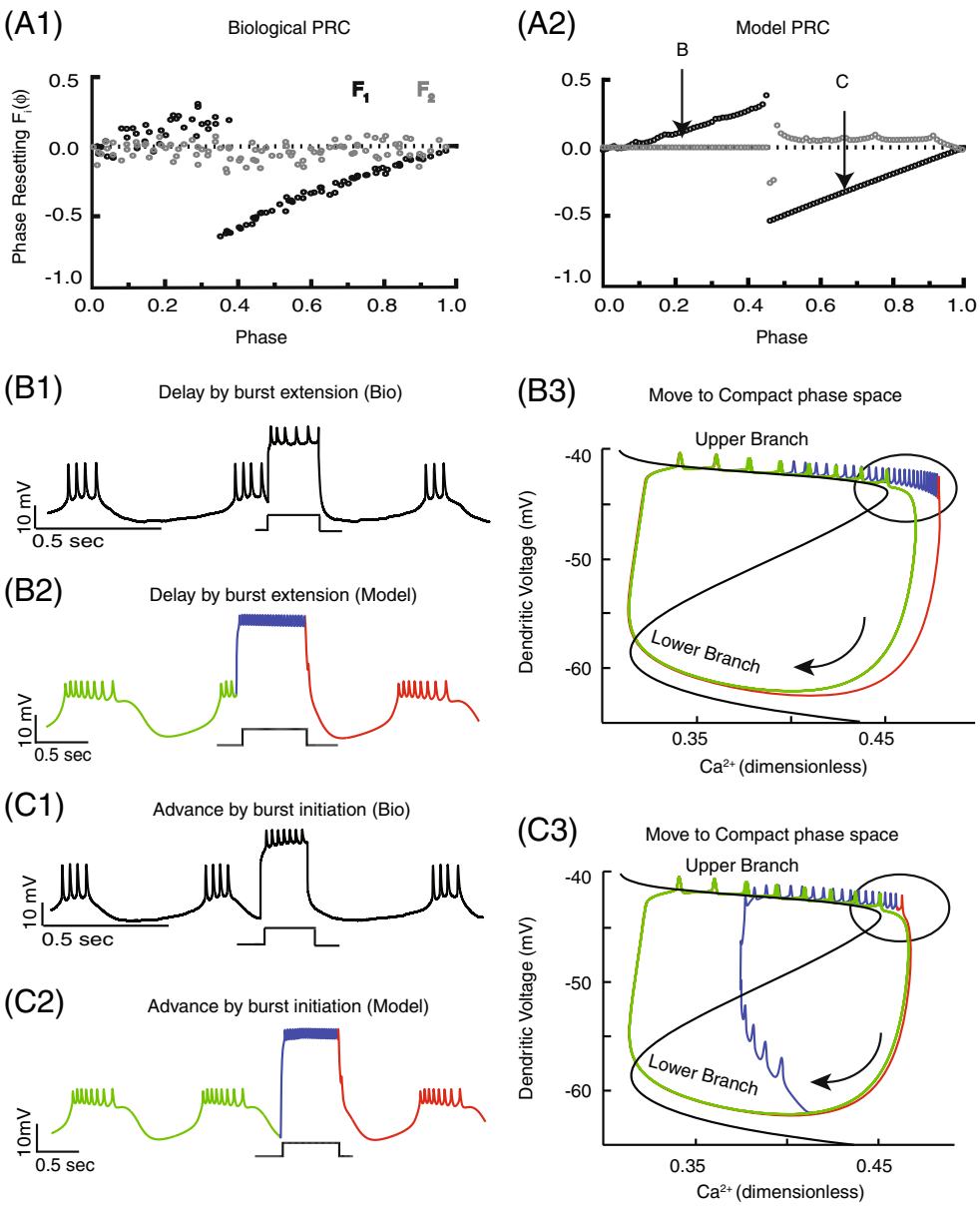

Fig. 5 Bilinear PRC for intermediate, strong pulses explained. (**A**) Biological (A1) and model (A2) PRCs, with first order in black and second order in gray. The arrows indicate the regions of the PRC that correspond to panels (B) and (C). (**B**) Voltage traces recorded at the soma for a pulse given during burst show delays due to burst extension for the biological (B1) and the model (B2) neuron. The black ovals in the dendritic phase plane diagrams (B3) correspond to a compact region of phase space to which the trajectory is confined until the end of the input. Spiking continues through the input pulse. (**C**) Voltage traces recorded at the soma for a pulse given during the interburst for the biological neuron (C1) and the model neuron (C2) show advances due to a burst initiated by the pulse. (C3) The dendritic phase plane analysis shows that a premature shift to the upper branch is maked by spiking during the pulse. The colors and curves in model neuron voltage trace and phase plane analysis correspond those in Fig. 3. In the model neuron, an input strength of 99 nS is applied for 650 ms. The biological neuron is Neuron 4 (G_{syn}=50 nS, duration=200 ms)

(I_{Ks}) in the model set to zero, then the model settles into tonic spiking if the pulse is left on indefinitely (Supplemental Figure 3(A3) and (A5). This compact region of phase space is a "ghost" of this tonically spiking attractor. Although I_{Ks} is not set to zero in this example, it is not significantly activated by an intermediate duration pulse, and the trajectory of the "ghost" spiking limit cycle is very compact compared to a bursting limit cycle, resulting in a nearly fixed rebound time, similar to what one would observe if the trajectory were consistently released from a fixed point in the phase space. Second order resetting is zero in this case because the second cycle follows the original limit cycle.

In contrast to pulses given during the burst, pulses given during the interburst (Fig. 5(C1) biological neuron and Fig. 5(C2) model neuron) produce an advance because the pulse initiates spiking almost immediately, such that the second linear segment of the PRC (Fig. 5(A1) and (A2)) approaches the causal limit. The input given during the interburst causes a transition to the upper branch to occur sooner (blue trace in Fig. 5(C3)) than for the unperturbed case (green trace in Fig. 5(C3)). In this case, the constant rebound (red trace) occurs during the second cycle after the perturbation and produces a constant, generally nonzero, F_2 for phases during the interburst (Fig. 5(A1) and (A2)). The transition to the upper branch in Fig. 5(C2) (and presumably Fig. 5(C1)) is obscured because the spiking during the transition to the upper branch is indistinguishable in the voltage trace from spikes that occur on the upper branch. Therefore the model is an invaluable tool to infer the dynamics underlying the observed phase resetting. The

distinction between whether spiking prolongs the existing burst or initiates a new one produces the apparent discontinuity in the bilinear PRC in both the biological neuron (Fig 5(A1)) and the model neuron (Fig. 5(A2)). Analytical expressions for the linear segments of the phase resetting curves are given in the summary section below.

3.4 U-shaped PRC

Long, weak pulses produce a roughly U-shaped first order PRC (Fig. 6(A1) and (A2)). Except for very early phases, in general conductance pulses produced only advancement in the first order PRC both the biological (Fig. 6(A1) black dots) and model neuron (Fig. 6(A2) black trace, with the region of advances indicated by the arrow labeled B). In both cases, the second order PRC consisted mostly of delays (gray dots). In the model, advances were produced mostly by shortening the interburst interval as shown in Fig. 6(B1) (biological neuron) and Fig. 6(B2) (model neuron). Especially when applied at late phases, the input also lengthens the burst in the next cycle, producing delays in F_2. The phase plane (Fig. 6(B3)) shows the advance results because during the pulse (blue trace) there is a premature switch to the upper branch, shortening the stay on the lower branch and hence the interburst. A longer burst in the first cycle also results from the three extra spikes at the end of the burst, but this is offset by the shorter interburst. The advance is most pronounced at intermediate phases when the depolarizing pulse extends throughout the interburst interval but does not lengthen the first burst.

3.5 Trilinear PRC

Strong long pulses produced trilinear PRCs (Fig. 7(A1) and (A2) in contrast to the bilinear PRCs produced by strong intermediate pulses. The salient difference is that longer pulses activate a second slow process, simulated in the model as I_{Ks} in the primary neurite, which in contrast to the case for intermediate pulses in Fig. 5, allows the trajectory to escape the compact area of phase space during tonic spiking at the end of a pulse (blue trace inside black oval in Fig. 7(B3)). Because the neuron escapes from the compact space, the recovery interval is no longer approximately constant. Furthermore, two line segments result rather than a single one for phases during a burst, depending upon whether the trajectory at pulse offset has crossed the separatix. For inputs given during the early burst (Fig. 7(B1)) biological and Fig. 7(B2) model), first order delays are produced by the prolongation of the burst due to continued spiking throughout the pulse. In this case, the trajectory of the model neuron (Fig. 7(B3)) is below the separatrix at pulse offset (end of blue trace, start of red). However, for inputs applied later in the burst (Fig. 7(C1)

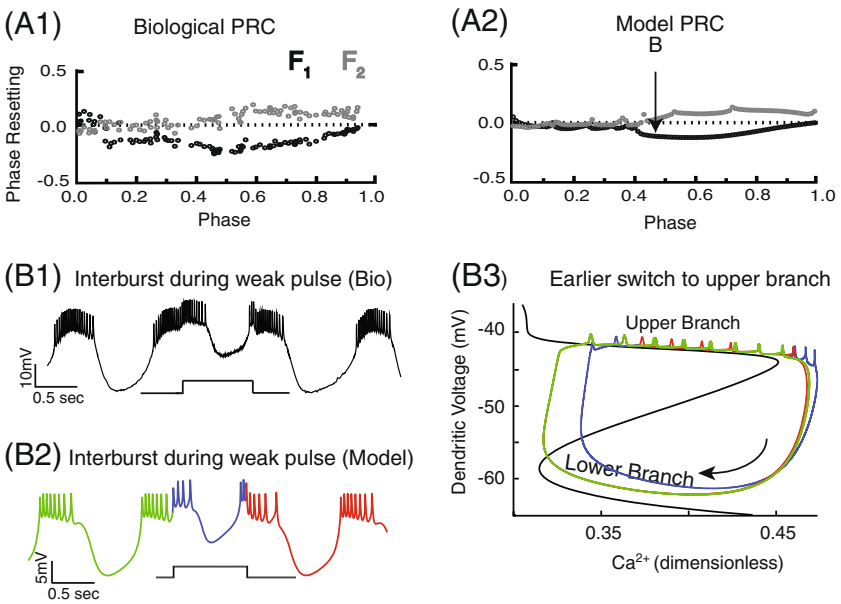

Fig. 6 'U' shaped PRC for long, weak pulses explained. (**A**) Biological (A1) and model (A2) PRCs, with first order in black and second order in gray. The arrow indicates the regions of the PRC that correspond to panel (B). (**B**) Voltage traces recorded at the soma for a pulse given during burst for the biological neuron (B1) and the model neuron (B2). An interburst interval occurs during the input. The biological neuron is Neuron 6 (G_{syn}=20 nS, duration=955 ms). In the model neuron, an input strength of 5 nS is applied for 1050 ms. Dendritic phase plane analysis (B3) shows that the transition to the lower branch occurs unimpeded during a weak pulse, followed by an earlier shift to the upper branch that produces an advance

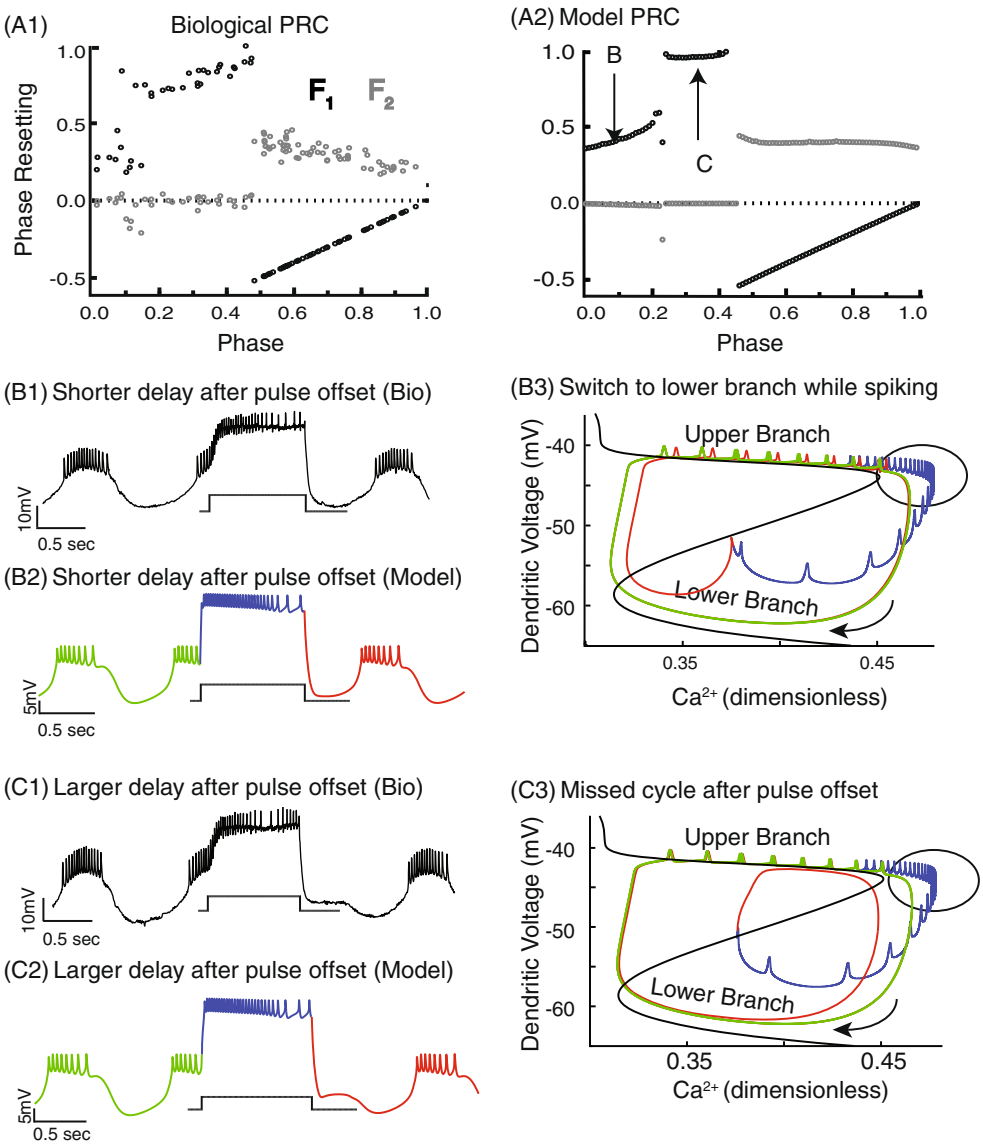

Fig. 7 Trilinear PRCs for long, strong pulses explained. (**A**) Biological (A1) and model (A2) PRCs, with first order in black and second order in gray. The arrows indicate the regions of the PRC that correspond to panels B and C. (**B**) Voltage traces recorded at the soma for a pulse during the early part of the burst exhibit short delays in the bio neuron (B1) and the model neuron (B2). The biological neuron is again Neuron 6 (G_{syn}=60 nS, duration= 955 ms). For the model neuron, an input strength of 50 nS is applied for 1,300 ms. (B3) The phase plane analysis shows that the trajectory is not confined to the upper branch during the pulse as it was for similar shorter inputs (Fig. 5(A3)) but instead continues spiking during the switch to the lower branch. (**C**) Voltage traces recorded at the soma for a pulse during the late part of the burst exhibit longer delays for the biological (C1) and model (C2) neuron. Dendritic phase plane analysis (C3) shows a missed cycle with no spiking on the upper branch that is responsible for the sharp increase in delays along the line segment labeled (C) in panel (A2). The colors and curves in model neuron voltage trace and phase plane analysis correspond to those in Fig. 3

biological neuron, Fig. 7(C2) model neuron), spiking still prolongs the burst, but the trajectory during the pulse (blue trace in Fig. 7(C3)) crosses the separatrix, allowing a premature jump (red trace compared to green trace in Fig. 7(C3)) to the upper branch. Moreover, the activation of the slow process is sufficient such that spiking cannot be maintained after pulse offset even though the trajectory is very close to the upper branch. This results in a "missed cycle" evidenced by a much longer delay in the second linear for phases between 0.2 and 0.4 in Fig. 7(A1) and (A2). The third and final linear segment has first order resetting at the causal limit and a nonzero F_2, similar to the final linear segment for the bilinear case. Although there were few instances of the trilinear PRC, the close correspondence between the biological (Fig. 7(A1)) and model (Fig. 7(A2)) PRCs is striking.

3.6 Summary of excitatory PRCs

Figure 8 summarizes schematically how the characteristic shape of the PRC changed as the strength and duration of the conductance pulse used to generate the PRC was varied. Tables 1 and 2 summarize the PRC data as well as the parameters of each experiment. Table 1 describes preparations in which synaptic inputs were given either as square pulses or synaptic conductance waveforms. Table 2 describes preparations that were given synaptic inputs as ramps. A total of 85 PRCs were generated in 12 biological neurons. Of the 85 PRCs, 24 (28.2%) had a prominent F_2 window, 12 (14.11%) were bilinear, 11 (12.94%) were cubic, 6 (7%) were trilinear, 4 (4.7%) were U-shaped, and 21 (24.7%) had negligible resetting (labeled nil in Fig. 8). There were also PRCs that fell into different categories

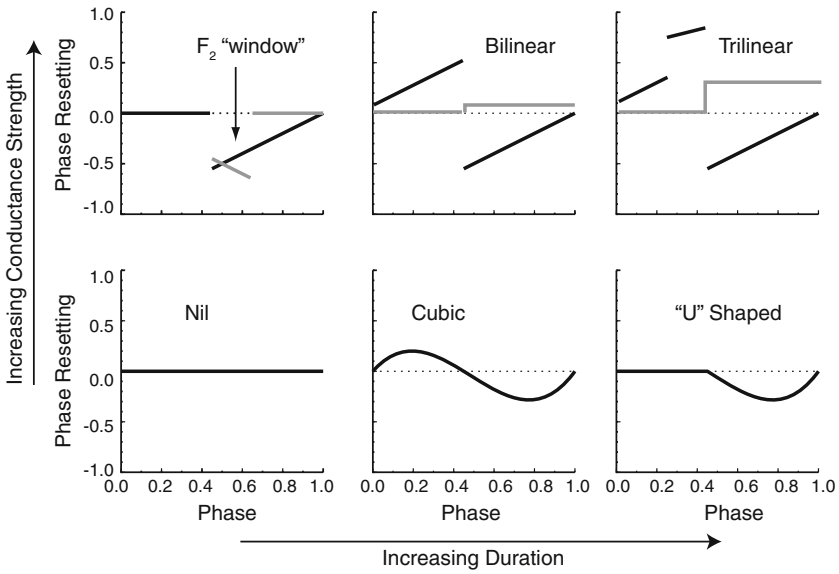

Fig. 8 Summary of the variation in observed PRC shapes. F_1 (*black*) is first order resetting and F_2 (*gray*) is second order resetting. The dependence of the characteristic shapes on the amplitude and duration of the excitatory conductance pulse is illustrated schematically. The prominent F_2 window and bilinear PRCs were generated using the equations in the text with the following parameters: ϕ_b=0.45, I_{dur}/P_0=0.35 and R/P_0=0.75

depending upon which phases were examined. These 7 transitional cases account for 8.23% of the total PRCs. The transitional cases result because there is a continuum of phase resetting behavior between the cases indicated in Fig. 8.

Simple equations characterize the PRC for the cases in which strong excitatory pulses reliably evoke spiking for the short and intermediate pulses, but not for the long pulses in which a secondary slow process confounds the analysis. These analyses given below focus only on explaining the PRC that is based on spiking observed at the soma, without explicit knowledge of the state of the burst generator. An analysis that includes the dynamics of the often unobservable branch switches in the burst generator and multiple bifurcations requires sophisticated mathematical analyses that will not be attempted here. However, in all cases, the match between the model and the observed PRCs is so striking we are confident that the model captures essential features of the dynamics of the AB/PD oscillator kernel.

The equations used to generate the schematic drawings for the prominent F_2 window and bilinear in Fig. 8 are given here; all other cases are illustrative and not based upon specific equations tied to the parameters of the dynamics and the stimulation pulse. For the prominent F_2 window case, the key insight is that the F_2 window arises when a short pulse occurs in the early part of the interburst interval. In this window alone, the spikes produced during the pulse are counted as a separate burst, because pulses at earlier phases overlap with the preceding burst and pulses given at later phases overlap with the next burst. The timing of the next burst is unchanged by the spikes during the pulse because the dynamics of the dendritic burst generator are unaffected, see Fig. 3. Therefore, the resetting is given by $F_1(\phi)=0$ for $\phi<\phi_b$ and $F_1(\phi)=\phi$ -1 for $\phi>\phi_b$ whereas $F_2(\phi)=0$ for $\phi<\phi_b$, $F_2(\phi)=-\phi$ for ($\phi>\phi_b$ and $\phi<1-I_{dur}/P_0$) and $F_2(\phi)=0$ for $\phi>1-I_{dur}/P_0$). The normalized burst duration is ϕ_b, the duration of the pulse is I_{dur} and P_0 is the intrinsic period. For the bilinear case, $F_1(\phi)=\phi + (I_{dur}+R-P_0)/P_0=\phi + A$ for $\phi<\phi_b$ and $F_1(\phi)=\phi$ -1 for $\phi>\phi_b$ whereas $F_2(\phi)=0$ for $\phi<\phi_b$ and $F_2(\phi)=A=(I_{dur}+R-P_0)/P_0$ for $\phi>\phi_b$, where the relaxation time back to the original limit cycle was assumed to be of constant duration R. The elapsed time from pulse onset to the next burst is the pulse duration plus the constant rebound, and the constant A is the normalized difference between this elapsed time and the intrinsic period. For pulse onset during a burst, A is the y-intercept of the linear segment, whereas for pulses given during the interburst, A is the constant second order resetting.

3.7 Inhibitory PRCs revisited

As stated in Section 1, a far simpler conceptual model of branch switching was able to account for phase resetting of the pyloric pacemaker kernel in response to inhibitory perturbations (Oprisan et al. 2003). Previously, short strong inhibitory pulses appeared to induce branch switching such that the amount of resetting could be predicted by assuming that switches between branches occur along a vertical line in the phase space corresponding to a constant value of the slow variable (Oprisan et al. 2003). The phase plane trajectories in Figs. 3(B2) and (C3) and 5(B3) and (C3) show that excitatory perturbations to the model may or may not switch the trajectory depending upon whether they cross the separatrix, and furthermore that whether a branch switch has occurred is not evident from examining the membrane potential trace alone. When we examined the

response to similarly short, strong inhibitory pulses, we found that the same principles apply. For short inhibitory pulses applied early during a burst (Fig. 9(A1) biological neuron and Fig. 9(A2) model neuron), the trajectory in the phase plane (Fig. 9(A3), blue trace) did not cross the separatrix during the pulse. A brief period of no spiking (beginning of red trace) was followed by a resumption of spiking on the upper branch. From the phase plane, it is evident that this is the continuation of the same burst. Nevertheless, in the experimental data, we have to be consistent in calling any resumption of spiking after a hyperpolarization a new burst because in the absence of measurements of slow variables we have no way to examine the phase space of the real neuron. For pulses applied later during the burst (Fig. 9(B1), biological neuron and Fig. 9(B2), model neuron), the trajectory (blue trace in Fig. 9B3) does indeed cross the separatrix, causing burst termination with a switch to the lower branch. Therefore the new model, in contrast to the old interpretation, predicts that the observed F_1 for inputs early during a burst (indicated by the arrow labeled A at phases up to about 0.1 in Fig. 9(C2)) will be qualitatively different than those observed later in a burst. A careful examination of the experimental data (Fig. 9(C1)) confirms this prediction in that the resetting at very early phases (up to about 0.05) appears to form a distinct cluster compared to the resetting observed from phases between 0.05 and 0.25, validating the new model. In order to match the experimental phase resetting for inhibitory cases, a fast outward current (I_{Kf}) that was activated by depolarization was added to the dendritic compartment. This current flattened the upper branch of the voltage nullcline to keep it close to the

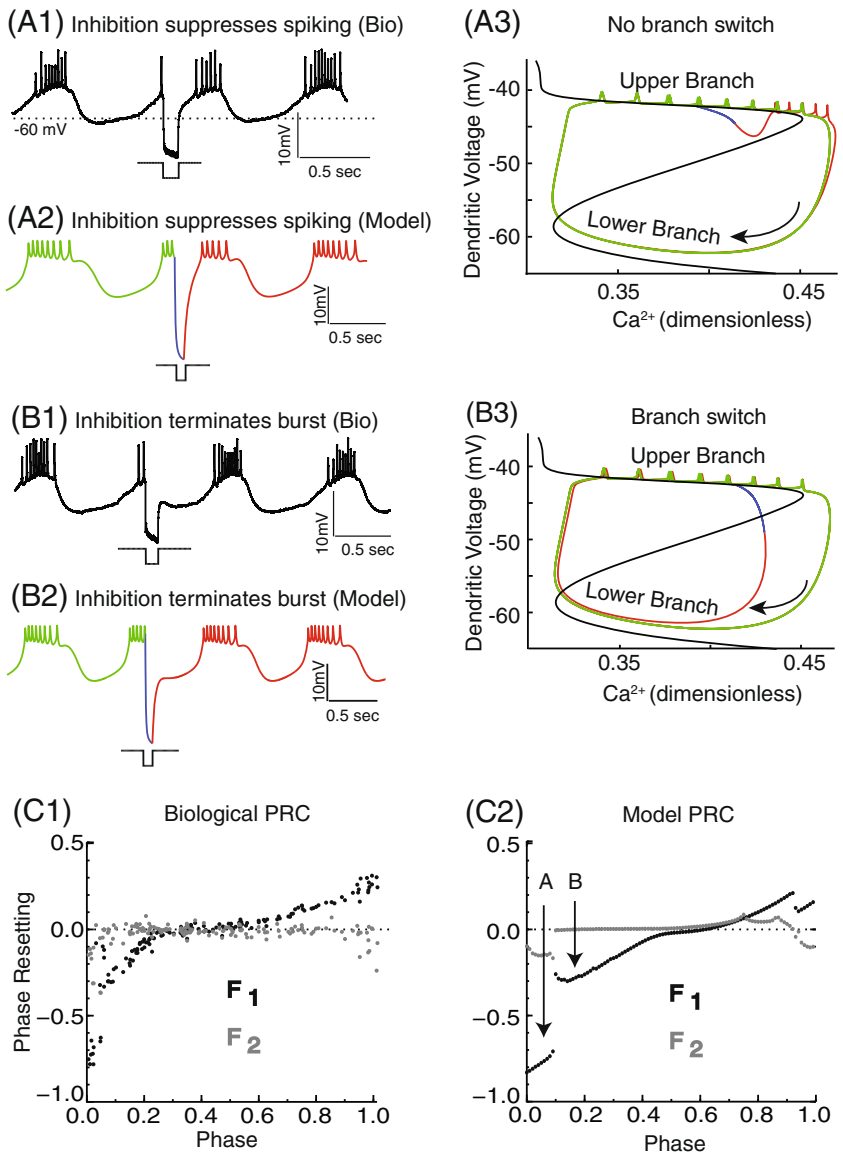

Fig. 9 Re-examination of resetting due to inhibitory inputs. (**A**) Spiking resumes quickly after pulse offset early in a burst for the biological (A1) and model (A2) neuron. A 400 nS inhibitory input was applied to the biological neuron for 150 ms. A 100 nS inhibitory input was applied to the biological neuron for 100 ms. The phase plane analysis (A3) shows that the burst after pulse offset is actually a continuation of the original burst, so there is no branch switch. The colors and curves in model neuron voltage trace and phase plane analysis correspond to those in Fig. 3. (**B**) Inhibition terminates the burst prematurely at slightly later phases than in A for both bio (B1) and model (B2) neuron. The phase plane analysis (B3) shows that the pulse terminates bursting by inducing a branch switch. (**C**) Phase response curves for the biological (C1) and model neuron (C2). F_1 (*black*) is first order resetting and F_2 (*gray*) is second order resetting. The arrows indicate the regions of large and small advances, respectively, that correspond to panels A and B respectively

separatrix, facilitating branch switches. The resultant PRCs (Fig. 9(C1)) match the experimental data (Fig. 9(C2)) better than our previous assumptions (Oprisan et al. 2003), and allow us to use a single model to reconcile phase resetting in response to both excitation and inhibition.

3.8 Dendritic versus somatic conductance injection

The reason that spikes can occur when the dendritic membrane potential is not on the upper branch is that spiking is initiated in the axon, and a strong depolarization of the soma can cause spiking in the axon without depolarizing the dendritic compartment sufficiently to induce a transition to the upper branch. We hypothesized that if the excitatory conductance were to be applied in the dendrites rather than in the soma, that spiking would once again correlate with movement on the upper branch of the dendritic potential nullcline. Since we are not able to inject the synaptic conductance in the dendrites of the AB/PD complex, we used the model to simulate this situation instead. A 50 nS conductance pulse was applied to the dendritic compartment instead of the somatic compartment (Fig. 10(A1) and (B1)), and the trajectories of model neuron during a perturbation (blue traces in Figs. 10(A2) and (B2)) became much more nearly vertical at a constant value of the slow variable, as expected for a relaxation oscillator (see Oprisan et al. 2003). For pulses applied both early (Fig. 10(A)) and late (Fig. 10 (B)) during the interburst, the PRC (Fig. 10(C)) became predictable in terms of observable switches between branches as we had initially anticipated. Therefore the spatial separation of the burst generator and conductance injection are critical to the resetting observed in the model, and likely in the biological neuron as well. Interestingly, small delays are observed when an excitation is applied during a burst (early phases Fig. 10(C)), consistent with experimental data (Benson 1980, see Section 4).

4 Discussion

In this study, PRCs were measured experimentally using the Dynamic Clamp to inject excitatory conductance pulses

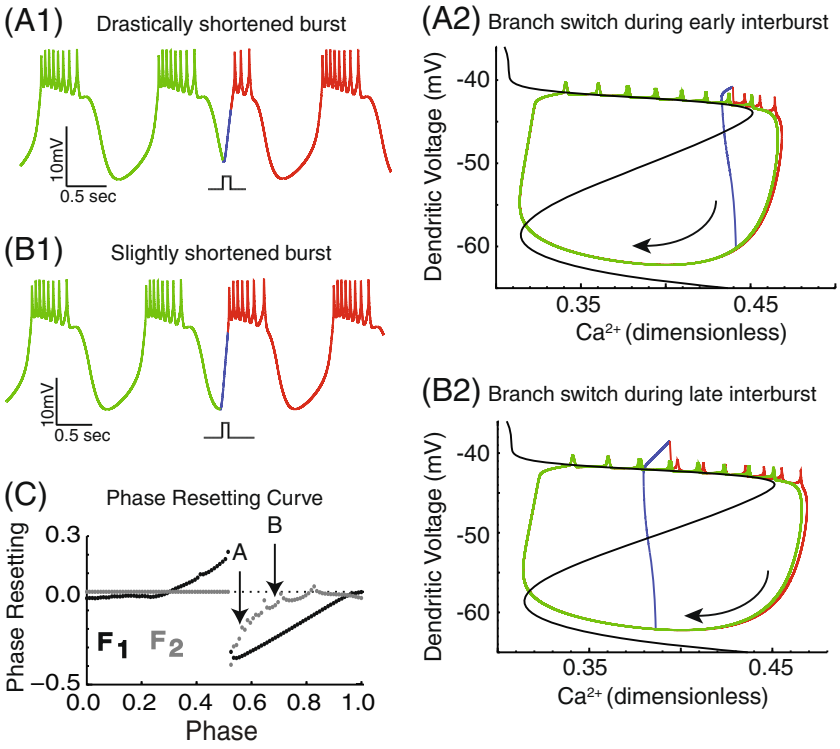

Fig. 10 Dendritic conductance injection. Strong short excitations given at the dendrite always cause branch switching. (**A**) Input given at the beginning of the interburst interval initiates a drastically shortened burst (A1). A 50 nS inhibitory input is applied for 100 ms. The phase plane analysis (A2) shows that an immediate transition to the upper branch results in the short burst. The colors and curves in model neuron voltage trace and phase plane analysis correspond to those in Fig. 3. (**B**) Input given in the middle of the interburst interval initiates a burst that is only slightly shortened (B1). The phase plane analysis (B2) shows why the burst following a branch switch is always shortened, and shortened more the earlier in the interburst that the input is applied. (**C**) Phase Response Curve, F_1 (*black*) is first order resetting and F_2 (*gray*) is second order resetting. The second order advances result from the shortened burst in the cycle following the perturbation, with the arrows indicating the regions that correspond to panels (A) and (B) respectively

of variable strength and duration into a PD soma of the pyloric pacemaker kernel. Based on the observed PRC shapes, five categories were identified (in addition to the nil PRC in which no resetting was observed). Of these five, the cubic and bilinear are probably most relevant to resetting that could occur in networks of bursting neurons, based on the assumption that the duration of a burst is the relevant time scale for synaptic perturbations in these circuits. However, the shorter and longer pulse durations helped to characterize the nonlinear dynamics of these neurons, and particularly to highlight the putative spatial segregation of oscillatory mechanisms for spiking versus burst generation. A model neuron with more than one compartment was required to reproduce all the types of PRCs that were observed. Phase plane analysis of the model clearly illustrated the mechanisms of phase resetting in the model neuron. Mechanisms underlying phase resetting of the model can be dissected with certainty, and the similarity of observed resetting in the model compared to the biological neuron allows us to infer by analogy that mechanisms for phase resetting are similar in the biological neuron. The model PRCs captured the essential trends of all PRC categories; therefore we propose that the interpretation of observed resetting in the model generalizes to the AB/PD complex and potentially to other bursting neurons as well, provided the burst generator is essentially a relaxation oscillator.

4.1 Interpretive value of model in the presence of spatial segregation

Here the beginning of a new burst is defined experimentally as the resumption of spiking after it has ceased. The presence of spiking would presumably be signaled to the downstream target, and there is at present no way to determine the status of the burst generator directly in an experiment. For these reasons, it seems logical and consistent to count every observable burst as a burst for the purposes of phase resetting, rather than ignoring "bursts" that are not linked to plateaus of the unobservable burst generator. The model presented here allows us to separate the spiking and bursting dynamics in a way that is not possible without it. The model led to a reinterpretation of our previous results for branch switching observed for short pulses at early phases in inhibitory neurons (Fig. 4 in Oprisan et al. 2003). Figure 9(A3) shows that a temporary cessation in spiking as demonstrated in Fig. 9(A2) does not always indicate burst termination and a branch switch. The main determinant of branch switching was whether the trajectory crossed the separatrix, or middle branch of the voltage nullcline, during the conductance pulse.

It is likely that the spatial segregation of the spiking mechanism from the burst generator may be more pronounced for excitation because a depolarizing pulse tends to open voltage gated channels and make the neuron less electrically compact, whereas a hyperpolarizing pulse tends to close channels and make the neuron more compact. Depending upon its localization, a depolarizing pulse, but not a hyperpolarizing one, can recruit ectopic spikes that complicate the interpretation of the data. The absence of clear switches of this nature in the biological neuron was puzzling until the model suggested that spiking alone was not an indicator of whether a switch to the upper branch was induced. For example, Figs. 3(B) and 5(B) do not indicate branch switches, whereas Figs. 3(C) and 5(C) do indicate such a switch. However, only the phase planes of the model (Figs. 3(B2), (C3), 5(B3) and (C3)) and not the voltage traces (Figs. 3(B1), (B3), (C1), (C2), 5(B1), (B2), (C1) and (C2)) reveal whether such a switch occurs. Since there is in every case an excellent correspondence between the shapes of the model and biological PRCs across all values of coupling strength and duration, we are confident that we can use this correspondence to infer when a branch switch has occurred in the biological neuron, even though they do not have the simple form predicted for the case in Fig. 10 in which the input is not spatially segregated from the burst generator. Thus, the phase resetting attributable to an input is strongly dependent upon the spatial localization (somatic vs dendritic) of the input, at least for excitation. This distinction between dendritic and somatic PRCs is based on access to the burst generating mechanism, and is quite different from those previously proposed mechanisms for distinct dendritic PRCs based on dendritic filtering (Goldberg et al. 2007) or activation of additional currents due to more rapid calcium accumulation in the dendrites (Schultheiss et al. 2010).

Previous models of the AB/PD complex have also included spatial segregation of spiking and burst generation (Soto-Treviño et al. 2005). All three somata in the PD complex (see Fig. 2(A)) are presumed to be electrically distant from the burst generator in the electrically coupled dendrites. This interpretation is supported by our observation that direct injection of the conductance pulses into the soma of AB (neuron 8 in Table 1) produced similar results compared to injection into the soma of PD (all other neurons). A gradual ramp (Table 2) was no more successful than a square pulse in inducing transitions. Two possible functional reasons for spatial segregation in general are metabolic efficiency or to give certain inputs preferential access to spiking versus burst generation depending upon the location of the synapse.

4.2 Role of second slow process

The large phase resetting observed during the latter portion of a burst for the trilinear PRCs (Fig. 7 (A1), phases from

0.2 to 0.4) required a second slow process (in addition to dendritic calcium accumulation). In order to simulate such a process, a slow voltage-activated potassium current that activates slowly at depolarized potentials, but de-activates more rapidly at hyperpolarized potentials was added to the primary neurite compartment. Rapid de-activation was required to allow full recovery; otherwise, a nonzero F_2 was obtained for the second linear segment of this PRC, in contradiction to the experimental data. The function of the slow K^+ current is to summate temporally during spiking to allow escape from the up branch (Fig. 7(B)) and in some cases to turn spiking off on the up branch (Fig. 7(C)) by countering the negative slope region in the IV curve. Not only did this current allow for escape from tonic spiking during a long pulse, but also during a very long conductance pulse this current allowed bursting to eventually be re-established in accordance with experimental observations (see Supplemental Figure 3(A2) and 3(A4) compared to 3(A3) and 3(A5), but see Soto-Treviño et al. 2005 for a counter-example). If this current is located in the same compartment as the burst generator then it counters the negative slope region due to the burst generating calcium current and shuts off bursting (Supplemental Figure 4) instead of spiking. Therefore in the model it is critical that the slow current must also be separated from bursting but not from spiking. This suggests that in the biological AB/PD complex, there is a strong homeostatic mechanism that favors bursting and acts over relatively short time scales (seconds) compared to other homeostatic mechanisms with longer time scales (Turrigiano et al. 1994, 1995). Hooper et al. (2009) use models and experimental data to argue that very slow conductances similar to our slow potassium conductance play an important role in maintaining phase constancy of bursting neurons in the pyloric circuit.

4.3 Inhibition is more reliable and a better choice for CPGs

Benson (1980) generated PRCs in the cardiac ganglion of the crab, *Portunus*, using current pulses rather than conductance pulses. Four small electrically coupled pacemaker neurons and five large follower motor neurons were considered as a single oscillatory kernel, and current was injected into the larger motor neurons. The phase resetting observed in response to inhibition was similar to that observed in our previous study of the AB/PD complex (Oprisan et al. 2003). For phase resetting in response to excitation, Benson found a "distinction between evoking action potentials, which occurred during depolarizing pulses of any duration of sufficient current intensity, and the induction of a driver potential and associated action potentials". This distinction seems to parallel the distinction we make between evoking action potentials and evoking a switch to the depolarized branch of the burst generator, hence the spatial separation between the two mechanisms may be general. Several cases were described depending upon the strength and timing of the pulse, not all of which correspond to cases that were observed in this study, which argues for the greater diversity of resetting in response to excitation compared to inhibition. For example, stronger pulses applied during a burst caused a premature termination of the burst at pulse offset, and the duration of the subsequent interburst interval was shorter (see Fig. 10(C)). Benson observed three types of responses to excitatory pulses given during the interburst interval: a brief pulse evoked no significant resetting, an intermediate pulse evoked a new burst that outlasted the input but was followed by a shortened interburst interval, and a long pulse evoked persistent spiking followed by a constant relaxation interval until the next burst. The intermediate responses were not observed in our experimental data (but were observed in the AB/PD model when current was injected into the dendrites, Fig. 10(A2) and (B2)). In our study, the longer pulses sometimes evoked a bursting pattern during the pulse rather than continuous spiking, and were sometimes but not always followed by a constant relaxation interval until the next burst.

Ayers and Selverston (1979) measured PRCs in the same bursting neurons utilized in the current study, the AB/PD complex of the lobster, but avoided the confounding effect of injecting current or conductance in the soma. Instead, the lateral pyloric (LP) neuron was stimulated in order to evoke inhibitory postsynaptic potentials and the inferior ventricular nerve (ivn) was stimulated to evoke excitatory postsynaptic potentials (EPSPs). In their preparations, neither the LP nor the ivn discharged spontaneously. The inhibitory PRCs were similar to those observed in our previous study (Oprisan et al. 2003), with early advances, an intermediate flat region, and late delays. The excitatory PRCs for a single EPSP was similar to our cubic PRC, and for twin facilitated EPSPs (a stronger input) the PRC was similar to our bilinear category. These PRCs consisted of early delays and late advances, with the caveat that the duration of their perturbations was short (less than 100 ms), so the extension of the burst that is responsible for early delays was not very noticeable. These experimentally derived PRCs could be simulated in the model by the injection of comparably brief pulses in the dendrites, or by longer pulses in the soma due to the spatial separation of the soma from the burst generator in the model.

In circuits of bursting neurons, the duration of the inhibition or excitation produced in the target of a bursting neuron is on the order of the burst duration, which is a significant fraction of the period. We have shown that the effect of excitation on a bursting neuron is much more variable and difficult to predict than that of inhibition,

therefore circuits of bursting neurons constructed using excitation may be less reliable that those based on inhibition (Sieling et al. 2009). This provides a possible explanation for why CPGs rely predominantly on inhibition. Excitation seems to also be more sensitive to the spatial location of the input (Fig. 10 and Supplemental Figure 3), which dictates caution in using the Dynamic Clamp to simulate synaptic connectivity. The AB/PD complex does not receive phasic excitation from the other components of the pyloric circuit *in vivo*, but our intent was to understand phase resetting generally in bursting neurons by using an easily accessible, easily isolated, and robust regular burster to explore the effects of resetting in bursting neurons due to excitatory pulses. Although excitatory synapses are not involved in generating the basic triphasic pyloric rhythm, pacemaker neurons do receive excitatory inputs from command fibers, which could modulate the triphasic rhythm. Dando and Selverston (1972) studied the effect of excitatory inputs on the pyloric rhythm by stimulating the ivn, which presumably activates dendritic synapses. They observed that at low stimulation frequency there is an increase in pyloric cycle frequency and at high frequency the endogenous bursting of pacemaker complex ceased, which is in agreement with our results for long dendritic inputs (Supplemental Figure 3(B)). For inhibitory pulses of burst durations in the range of those actually observed in this circuit, injection of the conductance in the soma adequately simulates the effect on phase resetting of a similar perturbation applied in the dendrites.

4.4 Effects of input strength and duration

A previous study (Prinz et al. 2003b) found that phase resetting in both the AB/PD complex and in an AB/PD model neuron due to both excitation and inhibition was independent of synaptic strength above a certain threshold but depended strongly upon duration. Oprisan et al. (2003) explained this dependence for inhibition by showing that longer inputs prevented a jump to the depolarized branch until their offset, at which time the neuron quickly shifted to the point on the depolarized branch of the limit cycle corresponding to burst initiation at a phase of zero. Here we demonstrated an analogous phenomenon for sufficiently strong excitatory inputs with intermediate duration. The main effect of input strength was whether action potentials were consistently evoked during the pulse or not. If they were, then the effect of duration was linear because the excitation increased the period by prolonging the burst as in the first segment of the bilinear PRC. However when the duration is further prolonged, unlike in the inhibitory case, in the case of excitation the neuron relaxed from the compact space.

4.5 Conclusion

In sum, five shapes of PRCs were observed in the AB/PD complex in response to somatic injection of artificial excitatory synaptic conductance pulses of different strengths and durations using the Dynamic Clamp. A four compartment model of the AB/PD complex with two slow processes produced a good match to all five PRC types, in addition to previous data on inhibition. In the model, spatial separation of spike and burst generation combined with a second slow process caused somatic spiking to be independent of the up and down states of the burst generator when the input is given at the soma. Phase plane analysis of the model allowed us to better understand switches between the upper and lower branches of the limit cycle that we propose generated the observed phase resetting. These methods can be generalized to apply to other bursters that rely on a slow process that may be spatially segregated from the point of observation and/or the locus for spike generation. Phase resetting of bursting neurons in response to excitation is much more complex than to inhibition, and the injection of excitatory synaptic conductances in the soma mimics dendritic activation less accurately than inhibitory. The variability is manifested differently but persists whether activation is dendritic or somatic (compare for example Fig. 10(A1) and (B1) to Fig. 3(B1) and (C1)). The major way in which this study relates to the pyloric circuit is to help explain why this circuit and similar circuits have evolved to rely on inhibition as being more reliable than excitation (see also Sieling et al. 2009).

Acknowledgements This work was supported by NIH grant NS054281 under the CRCNS program. We thank Ryan Hooper for supplying some of the PRCs and Rob Butera for comments on an earlier draft.

Appendix A: Model description

The model consists of four compartments. Each compartment obeys the following current balance equations,

$$C_m \frac{dv_s}{dt} = -\left(I_{syn} + I_{L,s} + I_{pn,s}\right)$$

$$C_m \frac{dv_{pn}}{dt} = -\left(I_{L,pn} + I_{Ks} - I_{pn,a} - I_{pn,d} - I_{pn,s}\right)$$

$$C_m \frac{dv_d}{dt} = -\left(I_{L,d} + I_{KCa} + I_{Ca} + I_A + I_{Kf} + I_{pn,d}\right)$$

$$C_m \frac{dv_a}{dt} = I_{ext} - \left(I_{L,a} + I_{Na} + I_{Kdr} + I_{pn,a}\right)$$

where V_s,V_{pn},V_d and V_a correspond to membrane voltage (mV) of soma, primary neurite, dendrite and axon respectively. C_m is the membrane capacitance and I_{ext} is a constant direct current.

1) The sodium current (I_{Na}) was taken directly from Guckenheimer et al. 1993 and is described by $I_{Na}= G_{Na}\ m^3h\ (V\text{-}E_{Na})$ where E_{Na} is the equilibrium potential for sodium and G_{Na} is the conductance strength. The activation variable m is set to the steady state value described by $m=\alpha_m/(\alpha_m+\beta_m)$.

$$a_m = \frac{\frac{127}{105}V+\frac{201}{7}}{10-10e^{-\frac{201}{70}-\frac{127}{1050}V}} \qquad b_m = 4e^{-\frac{188}{63}-\frac{127}{1890}V}$$

The inactivation variable h is described by the first order kinetics as follows.

$$\frac{dh}{dt} = \lambda_h(a_h(1-h)) - b_h h$$
$$a_h = \frac{7}{100}e^{-\frac{94}{35}-\frac{127}{2100}V}$$
$$b_h = \frac{1}{1+e^{-\frac{83}{35}-\frac{127}{1050}V}}$$

2) The delayed rectifier potassium current (I_{Kdr}) was taken directly from Guckenheimer et al. 1993 and is described by $I_{Kdr}=G_{Kdr}\ n^4\ (V\text{-}E_K)$, where G_{Kdr} is the conductance strength. The activation variable n is described by the following equations.

$$\frac{dn}{dt} = \lambda_n(a_n(1-n)) - b_n n$$
$$a_n = \frac{\frac{127}{105}V+\frac{166}{7}}{100-100e^{-\frac{83}{35}-\frac{127}{1050}V}}$$
$$b_n = \frac{1}{8}e^{-\frac{59}{140}-\frac{127}{8400}V}$$

3) The transient outward potassium current I_A was taken directly from Guckenheimer et al. 1993 and is described by $I_A=G_A\ m_A^3\ h_A\ (V\text{ - }E_K)$. The conductance G_A was set within the range studied by Guckenheimer et al. 1993. The activation variable m_A was set to its steady state value.

$$m_A = \frac{1}{1+e^{\frac{V-v_A}{sa}}}$$

The kinetics of the inactivation variable h_A are given by

$$\frac{dh_A}{dt} = (h_{Ai}-h_A)k_A \qquad h_{Ai} = \frac{1}{1+e^{\frac{v-v_b}{sb}}}$$

4) The slowly voltage-activated and calcium-inactivated calcium current (I_{Ca}) was taken directly from Guckenheimer et al. 1993, except τ_z was reduced from 23.5 to 23 ms, and is described by $I_{Ca} = G_{Ca}\ \frac{z}{0.43+c}\ (V-E_{Ca})$where E_{Ca} is the equilibrium potential for calcium, G_{Ca} is the conductance strength and c is the dimensionless calcium concentration whose kinetics are described below. The activation variable z is described by the following kinetic equations.

$$\frac{dz}{dt} = \frac{z_v-z}{\tau_z} \qquad z_v = \frac{1}{1+e^{-\frac{15}{100}(V-z_b)}}$$

5) The calcium-dependent potassium current (I_{KCa}) was taken directly from Guckenheimer et al. 1993 and is described by

$$I_{KCa} = G_{KCa}\ \frac{c}{0.5+c}\ (V-E_K)$$

where G_{KCa} is the conductance strength, which was set within the range studied by Guckenheimer et al. 1993.

6) The kinetics of the dimensionless activity of the free Ca^{2+} in the cytosol c were taken directly from Guckenheimer et al. 1993 except that ρ was changed from 0.003 ms^{-1} to 0.0016 ms^{-1}. They are described by the first order equation

$$\frac{dc}{dt} = \rho\left(\frac{k_{ca}z(v_{ca}-V)}{(1+2c)} - c\right).$$

7) The leak currents $I_{L,s}$, $I_{L,pn}$, $I_{L,d}$, $I_{L,a}$ in different compartments are given by $I_{Lj}=G_{Lj}\ (V_j\ \text{-}E_L)$, where $G_{L,j}$ is the leak conductance strength for different compartments. The reversal potential for this current was taken from Guckenheimer et al. 1993, but the conductances were adjusted to fit the PRC data using the compartmental model.

8) I_{ext} is an external bias current also used in the Guckenheimer model.

9) The very slow potassium current (I_{Ks}) in the primary neurite was not in the Guckenheimer et al. model, but its existence is supported by Hooper et al. 2009. We used the following description: $I_{Ks}=G_{Ks}\ p\ (V\text{ - }E_K)$, where E_k is the equilibrium potential for potassium and G_{Ks} is the conductance strength. The activation variable p is described by the following first order kinetics,

$$\frac{dp}{dt} = \frac{p_v-p}{\tau_{pV}}$$
$$p_v = \frac{1}{1+e^{-2.0(v+45.0)}}$$
$$\tau_{pV} = \frac{3000}{1+e^{\frac{-(v+50)}{0.05}}} + 100$$

10) The fast potassium current (I_{Kf}) was added in the dendrite to better match the shape of the burst envelope. It indicates an incomplete description of the existing potassium currents in the model and is given by $I_{Kf}=G_{Kf}\ b\ (V\text{ - }E_K)$, with conductance

strength given by G_{Kf}. The activation variable b is given by the following first order kinetics,

$$\frac{db}{dt} = \frac{b_v - b}{\tau_b} \qquad b_v = \frac{1}{1+e^{-2.0(v+42.0)}}$$

11) The coupling currents $I_{pn,d}$, $I_{pn,a}$, and $I_{pn,s}$ between soma(s), primary neurite (pn), axon (a) and dendrite (d) were introduced as a consequence of the multicompartmental model and are described by the following equations, $I_{pn,j}=G_{pn,j}$ (V_j - V_{pn}), where $j=s$, d or a for soma, dendrite or axon, respectively, where $G_{pn,j}$ is the coupling conductance strength between different compartments, set in order to separate compartments as required to reproduce the PRC data.

12) The synaptic current that simulates the virtual conductance applied at the soma is $I_{syn}=G_{syn}$ (V-E_{syn}) with synaptic conductance G_{syn} and reversal potential E_{syn}. Square pulses with G_{syn} of different strengths and durations were used to obtain representative PRCs.

References

Abbott, L. F., Marder, E., & Hooper, S. L. (1991). Oscillating networks: control of burst duration by electrically coupled neurons. *Neural Computation, 3*, 487–497.

Arshavsky, Y. I., Deliagina, T. G., Orlovsky, G. N., & Panchin, Y. V. (1989). Control of feeding movements in the pteropod mollusk, clione-limacina. *Experimental Brain Research, 78*, 387–397.

Arshavsky, Y. I., Grillner, S., Orlovsky, G. N., & Panchin, Y. V. (1991). Central generators and the spatiotemporal pattern of movements. In J. Fagard & P. H. Wolff (Eds.), *The development of timing control and temporal organization in coordinated action: Invariant relative timing, rhythms, and coordination* (pp. 93–115). Amsterdam: Elsevier.

Ayers, J. L., & Selverston, A. I. (1979). Monosynaptic entrainment of an endogenous pacemaker network: a cellular mechanism for von Holst's magnet effect. *Journal of Comparative Physiology, 129*, 5–17.

Benson, J. A. (1980). Burst reset and frequency control of the neuronal oscillators in the cardiac ganglion of the crab, Portunus sanguinolentus. *The Journal of Experimental Biology, 87*, 285–313.

Bucher, D., Johnson, C. D., & Marder, E. (2007). Neuronal morphology and neuropil structure in the stomatogastric ganglion of the lobster, Homarus americanus. *The Journal of Comparative Neurology, 501*(2), 185–205.

Calabrese, R. L., & Peterson, E. L. (1983). Neural control of heartbeat in the leech, *hirudo medicinalis*. In A. Roberts & B. Roberts (Eds.), *Neural origin of rhythmic movements* (pp. 195–221). Cambridge: Cambridge Univ. Press.

Canavier, C. C., & Achuthan, S. A. (2010). Pulse coupled oscillators and the phase resetting curve. *Mathematical Biosciences, 226*, 77–96. [Epub ahead of print] PMID: 20460132.

Cangiano, L., & Grillner, S. (2005). Mechanisms of rhythm generation in a spinal locomotor network deprived of crossed connections: the lamprey hemicord. *The Journal of Neuroscience, 25*, 923–935.

Cheng, J., Stein, R. B., Jovanovic, K., Yoshida, K., Bennett, D. J., & Han, Y. (1998). Identification, localization, and modulation of neural networks for walking in the mudpuppy (necturus maculatus) spinal cord. *The Journal of Neuroscience, 18*, 4295–4304.

Dando, M. R., & Selverston, A. I. (1972). Command fibres from the supra-oesophageal ganglion to the stomatogastric ganglion in *Panulirus argus*. *Journal of Comparative Physiology, 78*, 138–175.

Demir S. S., Butera, R. J. Jr., DeFranceschi A. A., Clark, J. W. Jr., & Byrne J. H. (1997). Phase Sensitivity and Entrainment in a Modeled Bursting Neuron. *Biophysical Journal, 72*, 579–594.

Dorval, A. D., Christini, D. J., & White, J. A. (2001). Real-time linux dynamic clamp: a fast and flexible way to construct virtual ion channels in living cells. *Annals of Biomedical Engineering, 29*, 897–907.

Ermentrout, G. B., & Kopell, N. (1991). Multiple pulse interactions and averaging in coupled neural oscillators. *Journal of Mathematical Biology, 29*(3), 195–217.

Glass, L., & Winfree, A. T. (1984). Discontinuities in phase resetting experiments. *The American Journal of Physiology, 246*(Regulatory Integrative Comp. Physiol. 15), R251–R258.

Goldberg, J. A., Deister, C. A., & Wilson, C. J. (2007). Response properties and synchronization of rhythmically firing dendritic neurons. *Journal of Neurophysiology, 97*(1), 208–219. Epub 2006 Sep 6.

Guckenheimer, J., Gueron, S., & Harris-Warrick, R. M. (1993). Mapping the dynamics of a bursting neuron. *Philosophical Transactions of the Royal Society of London. Series B: Biological Sciences, 341*, 345–359.

Hammond, C., Bergman, H., & Brown, P. (2007). Pathological synchronization in Parkinson's disease: networks, models and treatments. *Trends in Neurosciences, 30*, 357–364.

Hartline, D. K. (1979). Pattern generation in the lobster (panulirus) stomatogastric ganglion. II. Pyloric network simulation. *Biological Cybernetics, 33*, 223–236.

Hartline, D. K., & Gassie, D. V. (1979). Pattern generation in the lobster (panulirus) stomatogastric ganglion.I. Pyloric neuron kinetics and synaptic interactions. *Biological Cybernetics, 33*, 209–222.

Hooper, S. L., Buchman, E., Weaver, A. L., Thuma, J. B., & Hobbs, K. H. (2009). Slow conductances could underlie intrinsic phase-maintaining properties of isolated lobster (Panulirus interruptus) pyloric neurons. *The Journal of Neuroscience, 29*, 1834–1845.

Huguenard, J. R., & McCormick, D. A. (2007). Thalamic synchrony and dynamic regulation of global forebrain oscillations. *Trends in Neurosciences, 30*, 350–356.

Marder, E., & Calabrese, R. L. (1996). Principles of rhythmic motor pattern generation. *Physiological Reviews, 76*, 687–717.

McCrea, D. A., & Rybak, I. A. (2008). Organization of mammalian locomotor rhythm and pattern generation. *Brain Research Reviews, 57*, 134–146.

Miller, J. P., & Selverston, A. I. (1982). Mechanisms underlying pattern generation in lobster stomatogastric ganglion as determined by selective inactivation of identified neurons. II. Oscillatory properties of pyloric neurons. *Journal of Neurophysiology, 48*, 1378–1391.

Nargeot, R., Baxter, D. A., & Byrne, J. H. (1997). Contingent-dependent enhancement of rhythmic motor patterns: an *in vitro* analog of operant conditioning. *The Journal of Neuroscience, 17*, 8093–8105.

Nargeot, R., Petrissans, C., & Simmers, J. (2007). Behavioral and *in vitro* correlates of compulsive-like food seeking induced by operant conditioning in Aplysia. *The Journal of Neuroscience, 27*, 8059–8070.

Netoff, T. I., Acker, C. D., Bettencourt, J. C., & White, J. A. (2005). Beyond two-cell networks: experimental measurement of neuronal responses to multiple synaptic inputs. *Journal of Computational Neuroscience, 18*(3), 287–295.

Oprisan, S. A., Thirumalai, V., & Canavier, C. C. (2003). Dynamics from a time series: can we extract the phase resetting curve from a time series? *Biophysical Journal, 84*, 2919–2928.

Oprisan, S. A., Prinz, A. A., & Canavier, C. C. (2004). Phase resetting and phase locking in hybrid circuits of one model and one biological neuron. *Biophysical Journal, 87*, 2283–2298.

Preyer, A. J., & Butera, R. J. (2005). Neuronal oscillators in *aplysia californica* that demonstrate weak coupling *in vitro*. *Physical Review Letters, 95*(13), 138103.

Prinz, A. A., Billimoria, C. P., & Marder, E. (2003a). Alternative to hand-tuning conductance-based models: construction and analysis of databases of model neurons. *Journal of Neurophysiology, 90*, 3998–4015.

Prinz, A. A., Thirumalai, V., & Marder, E. (2003b). The functional consequences of changes in the strength and duration of synaptic inputs to oscillatory neurons. *The Journal of Neuroscience, 23*, 943–954.

Prinz, A. A., Abbott, L. F., & Marder, E. (2004). The dynamic clamp comes of age. *Trends in Neurosciences, 27*, 218–224.

Rinzel, J., & Ermentrout, B. (1989). Analysis of neural excitability and oscillations. In C. Koch & I. Segev (Eds.), *Methods in neuronal modelling: From synapses to networks"*. Cambridge: MIT. revised 1998.

Schultheiss, N. W., Edgerton, J. R., & Jaeger, D. (2010). Phase response curve analysis of a full morphological globus pallidus neuron model reveals distinct perisomatic and dendritic modes of synaptic integration. *The Journal of Neuroscience, 30*(7), 2767–2782.

Sharp, A. A., O'Neil, M. B., Abbott, L. F., & Marder, E. (1993a). Dynamic Clamp: computer-generated conductances in real neurons. *Journal of Neurophysiology, 69*, 992–995.

Sharp, A. A., O'Neil, M. B., Abbott, L. F., & Marder, E. (1993b). The dynamic clamp—Artificial conductances in biological neurons. *Trends in Neurosciences, 16*, 389–394.

Sieling, F. H., Canavier, C. C., Prinz, A. A. (2009). Predictions of phase-locking in excitatory hybrid networks: excitation does not promote phase-locking in pattern generating networks as reliably as inhibition. *J Neurophysiol*, *102*, 69–84. First published doi:10.1152/jn.00091.2009.

Soto-Treviño, C., Rabbah, P., Marder, E., & Nadim, F. (2005). Computational model of electrically coupled, intrinsically distinct pacemaker neuron. *Journal of Neurophysiology, 94*, 590–604.

Stein, S. G., Grillner, S., Selverston, A. I., & Stuart, D. G., (Eds). (1997). *Neurons, networks, and motor behavior.* MIT.

Tazaki, K., & Cooke, I. M. (1990). Characterization of Ca current underlying burst formation in lobster cardiac ganglion motor-neurons. *Journal of Neurophysiology, 63*, 370–384.

Tohidi, V., & Nadim, F. (2009). Membrane resonance in bursting pacemaker neurons of an oscillatory network is correlated with network frequency. *The Journal of Neuroscience, 29*, 6427–6435.

Traub, R. D., & Jefferys, J. G. (1994). Are there unifying principles underlying the generation of epileptic afterdischarges *in vitro*? *Progress in Brain Research, 102*, 383–394.

Turrigiano, G., Abbott, L. F., & Marder, E. (1994). Activity-dependent changes in the intrinsic properties of cultured neurons. *Science, 264*(5161), 974–977.

Turrigiano, G., LeMasson, G., & Marder, E. (1995). Selective regulation of current densities underlies spontaneous changes in the activity of cultured neurons. *Journal of Neuroscience, 15*(5 Pt 1), 3640–3652.

Winfree, A. T. (1980). *The geometry of biological time*. New York: Springer.